Biogeosciences

Beyond the Fe-P-redox connection: preferential regeneration of phosphorus from organic matter as a key control on Baltic Sea nutrient cycles

T. Jilbert[1], C. P. Slomp[1], B. G. Gustafsson[2], and W. Boer[3]

[1]Department of Earth Sciences (Geochemistry), Faculty of Geosciences, Utrecht University, P.O. Box 80.021, 3508 TA Utrecht, The Netherlands
[2]Baltic Nest Institute, Stockholm Resilience Centre, Stockholm University, 106 91 Stockholm, Sweden
[3]Royal Netherlands Institute for Sea Research (NIOZ), P.O. Box 59, Den Burg, Texel, The Netherlands

Abstract. Patterns of regeneration and burial of phosphorus (P) in the Baltic Sea are strongly dependent on redox conditions. Redox varies spatially along water depth gradients and temporally in response to the seasonal cycle and multidecadal hydrographic variability. Alongside the well-documented link between iron oxyhydroxide dissolution and release of P from Baltic Sea sediments, we show that preferential remineralization of P with respect to carbon (C) and nitrogen (N) during degradation of organic matter plays a key role in determining the surplus of bioavailable P in the water column. Preferential remineralization of P takes place both in the water column and upper sediments and its rate is shown to be redox-dependent, increasing as reducing conditions become more severe at greater water-depth in the deep basins. Existing Redfield-based biogeochemical models of the Baltic may therefore underestimate the imbalance between N and P availability for primary production, and hence the vulnerability of the Baltic to sustained eutrophication via the fixation of atmospheric N. However, burial of organic P is also shown to increase during multidecadal intervals of expanded hypoxia, due to higher net burial rates of organic matter around the margins of the deep basins. Such intervals may be characterized by basin-scale acceleration of all fluxes within the P cycle, including productivity, regeneration and burial, sustained by the relative accessibility of the water column P pool beneath a shallow halocline.

1 Introduction

Hypoxia has been intermittently present in the Baltic Sea throughout the Holocene (Zillen et al., 2008), but its severity and spatial extent have increased greatly over the past 100 years (Conley et al., 2009a; Fonselius and Valderrama, 2003; Jonsson et al., 1990). This has led to multiple ecological impacts, such as the disruption of benthic foodwebs (Karlson et al., 2005) and fish habitats (Cardinale and Modin, 1999). Rising anthropogenic nutrient loadings in the early 20th century are believed to have provided the initial trigger to the modern eutrophication of the Baltic, with the resulting increased biological oxygen demand forcing the exacerbation of hypoxia (Savchuk et al., 2008). However, both eutrophic conditions and hypoxia have persisted to the present day, despite a decline in fertilizer use in the catchment since the 1990s (Emeis et al., 2000). Natural feedbacks within the cycles of phosphorus (P) and nitrogen (N) in low-oxygen systems (Middelburg and Levin, 2009) likely play a key role in allowing the Baltic to self-sustain hypoxia. Regeneration of P as phosphate (HPO_4^{2-}) is known to be enhanced from sediments underlying hypoxic or anoxic bottom waters. Phosphate is released during the remineralization of organic matter, and the rate of P remineralization may accelerate relative to that of carbon and nitrogen during anaerobic degradation (Ingall et al., 1993). Additionally, the dissolution of P-bearing Fe-oxyhydroxides in surface sediments increases the rate of P regeneration during the transition into hypoxia or anoxia (Einsele, 1936; Mortimer, 1941, 1942) . On the other hand, nitrification and denitrification rates may also vary as oxygen is depleted (Kemp et al., 1990). Basin-scale

biogeochemical modeling of the Baltic Proper through the last century shows the net result of altered anthropogenic nutrient loading and oxygen-dependent feedbacks to be an excess of phosphate in the modern water column (Savchuk et al., 2008). This situation stimulates the fixation of atmospheric N by cyanobacteria (Vahtera et al., 2007), maintaining high primary productivity in the basin. In turn, decay of sinking biomass maintains hypoxia in the bottom waters, providing the conditions for ongoing phosphate regeneration from the sediments.

Within the context of a generally eutrophied, hypoxic modern Baltic, the spatial distribution of hypoxia is controlled by the physical characteristics of the water column (Fonselius, 1981). In the Baltic Proper, a persistent stratification exists between surface waters of salinity 7–8 and bottom waters of salinity 11–13, the latter generated by major inflows across the Danish Straits (Matthaus and Franck, 1992; Meier et al., 2006; Schinke and Matthaus, 1998). Vertical profiles of salinity and dissolved oxygen throughout the basin are strongly anti-correlated, with a mid-depth halocline marked by a steep decline in oxygen (Fonselius, 1981), across which turbulent diffusive exchange is limited (Gustafsson and Stigebrandt, 2007). The frequency of major saline inflows affects the spatial extent of hypoxia by determining the depth and gradient of the halocline. During stagnations (i.e. the multiannual periods between major inflows), the halocline may be eroded vertically, reducing the total area of bottom-water hypoxia. New inflows then reestablish a strong halocline, allowing bottom water hypoxia to spread (Gustafsson, 2000). Major inflows always occur during winter westerly storms across the Danish Straits, but their frequency has reduced dramatically from nearly annual in the early to mid- 20th century to roughly decadal since 1983 (Schinke and Matthaus, 1998), with the most recent occurring in 2003. This change in frequency of major inflows is believed to result from the relative weakness of easterly winds in the early winter "preconditioning" phase during recent decades (Lass and Matthaus, 1996), and has led to high-amplitude variability in the area of hypoxic bottom waters during this period (Conley et al., 2002). The size of the hypoxic area also displays a large seasonal fluctuation due to oxygen consumption after the spring-summer phytoplankton bloom (Conley et al., 2002).

Given the coupling between hypoxia and nutrient cycles, the strong physically-driven variability in bottom water hypoxia during the inflow-stagnation cycle may be expected to influence regeneration and burial of nutrients on the basin-scale, and hence to influence nutrient budgets of the Baltic (Gustafsson and Stigebrandt, 2007; Savchuk and Wulff, 2009). In the case of P, it has been proposed that sediments in the Baltic Proper act as a net source of phosphate during expansion of the hypoxic area, as Fe-oxyhydroxides at the sediment surface are reductively dissolved in the absence of oxygen (Conley et al., 2002). Conversely, the opposite should be true as the hypoxic area contracts, namely that the

sediments become a net sink for P. In accordance with this theory, the basin-scale modeling approach of Savchuk and Wulff (2009) considers a linear enhancement of P regeneration with expansion of the hypoxic area. Similarly, Gustafsson and Stigebrandt (2007) assume the uptake or release of P by sedimentary iron oxyhydroxides to account for any deviation in water column phosphate concentrations away from the value predicted by remineralization of organic matter in Redfield proportions. However, the behavior of phosphorus in Baltic Sea sediments has only recently begun to be studied in detail (Hille et al., 2005; Lukkari et al., 2009; Mort et al., 2010), and a large amount remains to be learned about the response of phosphorus regeneration, and burial, to spatial and temporal hydrographic variability. In particular, the respective roles of the iron oxyhydroxide-P (or "Fe-P") interaction, and preferential remineralization of P during anaerobic degradation of organic matter, are poorly constrained. Although some recent models, such as BALTSEM of the Baltic Nest Institute in Stockholm, include preferential remineralization of P from organic matter as a process (Oleg Savchuk, personal communication, 2011), a lack of comprehensive geochemical data hinders validation of its magnitude. The present study aims to address this issue. Firstly, we investigate the characteristics of P regeneration during the current stagnation using a broad network of sediment and porewater profiles throughout the Baltic Proper and the Gulf of Finland. We adopt a water-depth based approach, to investigate the contrasting behavior of sites along the redox gradient into the deep basins. Secondly, we investigate the response of P burial to the inflow-stagnation cycle by studying the accumulation rate of P in ^{210}Pb-dated sediment cores. The results allow a re-examination of existing theories about the relationship between hypoxia and the phosphorus cycle in the Baltic.

2   Materials and methods

2.1   Onboard sampling and analyses

A total of 17 sites in the Baltic Proper and Gulf of Finland, covering a range of water depths, were visited during the HYPER/COMBINE cruise of the R/V *Aranda* in May/June 2009 (Fig. 1). Water column salinity and dissolved oxygen profiles were measured using a CTD system, and additional bottom-water oxygen concentrations were measured by Winkler titration. A multicorer retrieving sub-cores of length ≤50 cm was deployed at each site. At 9 sites, a bottom water sample was taken from one sub-core using a 20 ml plastic syringe, and transferred immediately to an anoxic glove box. The same sub-core was inserted into the glove box through an air-tight hole in the base and the remaining bottom water was removed. The sub-core was then sliced at a resolution of 0.5 cm (0–2 cm depth), 1 cm (2–10 cm depth) and 2 cm (>10 cm depth). An aliquot of each wet sediment
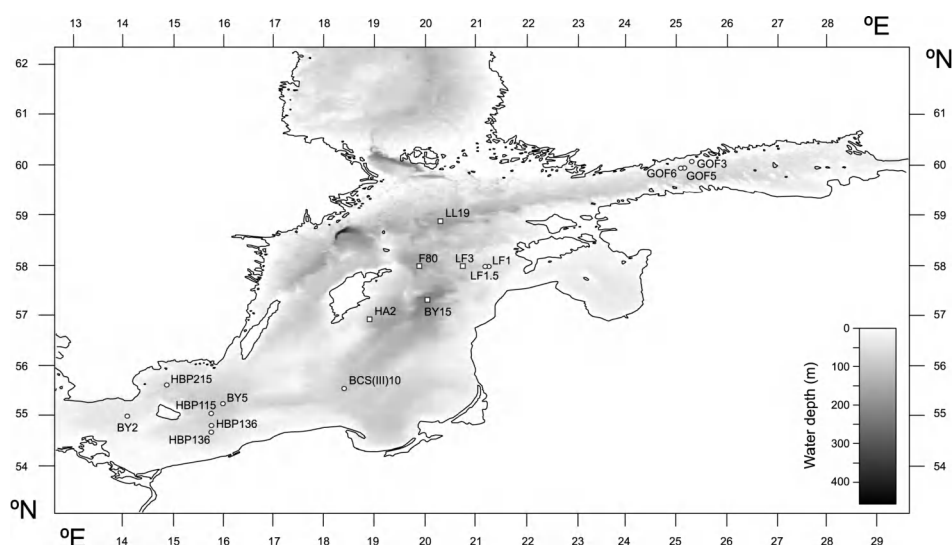
Fig. 1. Bathymetric map of the Baltic Proper, showing the locations of the coring sites used in this study. Circles represent Group 1 sites ($\leq$90 m water depth), squares represent Group 2 sites (>90 m water depth). Bathymetric and coastline data are presented in equidistant cylindrical projection, taken from the General Bathymetric Chart of the Oceans (GEBCO) Digital Atlas (Intergovernmental Oceanographic Commission et al., 2003).

sample was transferred to a 50 ml plastic centrifuge tube, which was capped, removed from the glove box and centrifuged at 2500 g for 10–30 min. The centrifuge tubes were then returned to the glove box. The supernatant water from each sample, including the bottom water sample, was dispensed via a 20 ml plastic syringe through a 0.45 μm filter and collected in a 15 ml plastic centrifuge tube. Subsamples were taken for analysis of dissolved phosphate and iron (acidified with 10 μl of 37 % HCl per ml of subsample and stored at 5 °C) and ammonium, nitrate and sulfate (stored at −20 °C). The remainder of each wet sediment sample was transferred to a pre-weighed 15 ml glass vial for solid-phase analyses. The vial was capped and stored in a nitrogen-filled airtight jar. At the remaining 8 sites, a bottom water sample was taken as above, and porewater samples were taken using rhizon samplers (Seeberg-Elverfeldt et al., 2005) from a sub-core pre-drilled with 3 mm diameter holes at 1 cm vertical spacing. The uppermost rhizon sample was taken from the first hole below the sediment water interface and was assumed to collect porewater from the upper 1 cm of sediment, centered on 0.5 cm depth. The rhizons were attached to 10 ml plastic syringes, which were allowed to fill with porewater (for 10–30 min) and transferred to the glove box for subsampling as above. Site BY2 was also visited during a cruise with the R/V *Skagerak* in September 2007 and sampled for porewater and solid-phase parameters as per the above protocols, with porewater extraction by centrifugation (Mort et al., 2010).

2.2 Laboratory analyses

Phosphate, ammonium and nitrate in porewater samples were determined spectrophotometrically using an Autoanalyser. Sulfate was determined using a Dionex Ion Chromatograph. Iron and other elements in porewaters were analyzed by Perkin Elmer Optima 3000 Inductively Coupled Plasma-Optimal Emission Spectroscopy (ICP-OES; all iron was presumed to be present as Fe^{2+}). Wet sediment samples from BY2, GOF3, GOF5, LF1, GOF6, LF1.5, LF3, LL19, F80 and BY15 were frozen within the airtight jars, then removed from the jars and freeze-dried to estimate water content. The dried sediment was transferred to an anoxic glove box and ground in an agate mortar. Aliquots of 0.5 g dried sediment were decalcified by shaking in excess 1 M HCl, initially for 12 h and for a further 4 h after addition of new acid. Tests have shown that the amount of organic carbon hydrolyzed by this protocol is negligible (van Santvoort et al., 2002). The decalcified sediment was dried, ground in an agate mortar and analyzed by combustion for organic carbon (C_{org}) and total nitrogen (N_{tot}) using a Fisons NA 1500 NCS (precision and accuracy <2 % based on an atropine/acetanilide standard calibration and checked against internal laboratory standard sediments). The non-organic contribution to N_{tot} is assumed negligible in these sediments, hence $N_{tot} \approx N_{org}$. A second 0.1 g aliquot of dried sediment was dissolved in 2.5 ml HF (40 %) and 2.5 ml of a $HClO_4/HNO_3$ mixture, in a closed Teflon bomb at 90 °C for 12 h. The acids were then evaporated at 190 °C and the resulting gel was dissolved in 1M HNO_3, which was analyzed for selected elemental concentrations by ICP-OES (precision and accuracy <5 %, based on calibration

to standard solutions and checked against internal laboratory standard sediments). A third 0.1 g aliquot was subjected to the SEDEX sequential extraction procedure to determine the solid-phase partitioning of phosphorus (Ruttenberg, 1992). All H_2O rinses were omitted from the original protocol (see Slomp et al., 1996), but three $MgCl_2$ rinses were included. The full speciation was as follows: exchangeable-P (extracted by $1M\ MgCl_2$, pH 8, 0.5 h), iron oxyhydroxide-bound P ("Fe-P", extracted by citrate-bicarbonate-dithionite (CDB), pH 7.5, 8 h, followed by $1M\ MgCl_2$, pH 8, 0.5 h), authigenic Ca–P (including carbonate fluorapatite, biogenic hydroxyapatite and $CaCO_3$-bound P, extracted by Na-acetate buffer, pH 4, 6 h, followed by $1M\ MgCl_2$, pH 8, 0.5 h), detrital Ca–P (extracted by 1 M HCl, 24 h) and organic P (P_{org}, after ashing at $550\,^\circ\mathrm{C}$ for 2 h, extracted by 1M HCl, 24 h). The initial $1M\ MgCl_2$ and CDB rinses were performed inside the anoxic glove box, to eliminate the potential conversion of authigenic Ca-P to Fe-P due to pyrite oxidation upon oxygen exposure (Kraal et al., 2009). Dissolved phosphate in all rinses was analyzed colorimetrically (Strickland and Parsons, 1972) on a Shimadzu Spectrophotometer (precision and accuracy $<2\,\%$, based on calibration to standard solutions and checked against internal laboratory standard sediments), with the exception of the CDB rinse, in which P and Fe were analyzed by ICP-OES. Only the P_{org} data (from all analyzed sites) and Fe-P data from BY2 (June and September) are presented in this paper. A fourth 0.1–0.5 g aliquot of dried sediment from sites LF1, LF1.5 and LF3 was reserved for ^{210}Pb analysis. This was spiked with [209]Po and digested in 10 ml concentrated HCl in a microwave oven for 3 h. 2 ml 3.5 % $HClO_4$ was then added and the acids were removed by evaporation. The resulting precipitate was redissolved in 5 ml concentrated HCl for 30 min. Thereafter, 40 ml 0.5 M HCl (with $12\,\mathrm{g\,l^{-1}}$ boric acid), 4 ml NH_4OH and 5 ml $40\,\mathrm{g\,l^{-1}}$ ascorbic acid (in 0.5 M HCl) were added. Po-isotopes were deposited by suspending silver disks in the solution, which was heated to $80\,^\circ\mathrm{C}$ for 4 h then left overnight at room temperature. The activity of [210]Po was measured by α-spectrometry with Canberra Passivated Implanted Planar Silicon (PIPS) detectors, allowing ^{210}Pb activity to be back-calculated. 1σ counting uncertainty was on average 5 %.

3   Results and discussion

3.1   Porewater profiles and regeneration fluxes

A complete overview of the water column and porewater data from the 17 sites sampled in May/June 2009, and site BY2 from September 2007 (Mort et al., 2010), is presented in Fig. 2 (raw porewater data is presented in Table A1). The sites range in water-depth from 48 m (BY2) to 238 m (BY15). For simplicity and synergy with Mort et al. (2010), we categorize all sites of <90 m depth as "Group 1 (oxic-seasonally hypoxic)", whereas sites of >90 m water depth

are categorized as "Group 2 (semi-permanently hypoxic-anoxic)". At the time of sampling in May/June 2009, all sites except BY2, LF1 and LF1.5 experienced bottom water oxygen concentrations below $2\,\mathrm{ml\,L^{-1}}$, hence were "hypoxic" as per the commonly adopted definition (Diaz and Rosenberg, 1995). The five Group 2 sites were anoxic, with hydrogen sulfide present in the water column (plotted in Fig. 2 as "negative oxygen" concentrations, as per Fonselius (1981)). The stratification control on water column oxygen concentration is clear from the inverse relationship between oxygen and salinity at all sites, although the depth and gradient of the halocline vary between and within sub-basins. Most sites display evidence for sulfate reduction in the porewaters, with complete removal of sulfate within the depth of the multicore at a number of sites. Porewater ammonium (NH_4^+) profiles at all sites show an asymptotic increase with depth, typical of NH_4^+ release during organic matter remineralization in sediments undisturbed by bioturbation (Burdige, 2006). The flux of NH_4^+ across the sediment-water interface, calculated from the concentration gradient between the bottom water and uppermost porewater sample, therefore provides a minimum estimate of the rate of organic matter remineralization at each site. Although the true rate of remineralization at sites with oxygen penetration into the sediments may be greater, due to the oxidation of ammonium to nitrate in the uppermost sample, very low porewater nitrate concentrations at these sites (not shown) and the strongly asymptotic NH_4^+ profiles suggest this effect to be negligible. Hence, the relationship between the porewater profiles and fluxes of NH_4^+, phosphate (HPO_4^{2-}) and iron (II) (Fe^{2+}) may justifiably be used to deconvolve regeneration of HPO_4^{2-} due to iron oxyhydroxide dissolution from regeneration due to remineralization of organic matter at the sites in this study.

Throughout both groups of sites, no clear trend is observed with water depth for absolute fluxes of NH_4^+ or HPO_4^{2-} (Fig. 2). This statement holds whether sites sampled with rhizons (marked "R" in Fig. 2, for which a greater degree of error is expected due to the difficulty in capturing the true concentration gradient across the sediment-water interface) are included or excluded. However, a marked depth-dependence is observed in the NH_4^+/HPO_4^{2-} flux ratio (Fig. 3a). Most striking is the cluster of Group 1 sites recording values of 0–3, while all Group 2 sites record values of 10–20. This distribution is explained by closer examination of the upper 10 cm of the porewater NH_4^+ and HPO_4^{2-} profiles at each site. Group 1 sites with NH_4^+/HPO_4^{2-} flux ratios of 0–3 display a peak of porewater HPO_4^{2-} in the shallow subsurface which is not replicated in NH_4^+ (Figs. 2, 3b). This peak causes the diffusive HPO_4^{2-} flux to exceed the value predicted by organic matter remineralization alone, suppressing the NH_4^+/HPO_4^{2-} flux ratio. Coincident peaks in Fe^{2+}, which drive non-zero diffusive fluxes of Fe^{2+} (Figs. 2, 3c), provide evidence that dissolution of P-bearing iron oxyhydroxides close to the
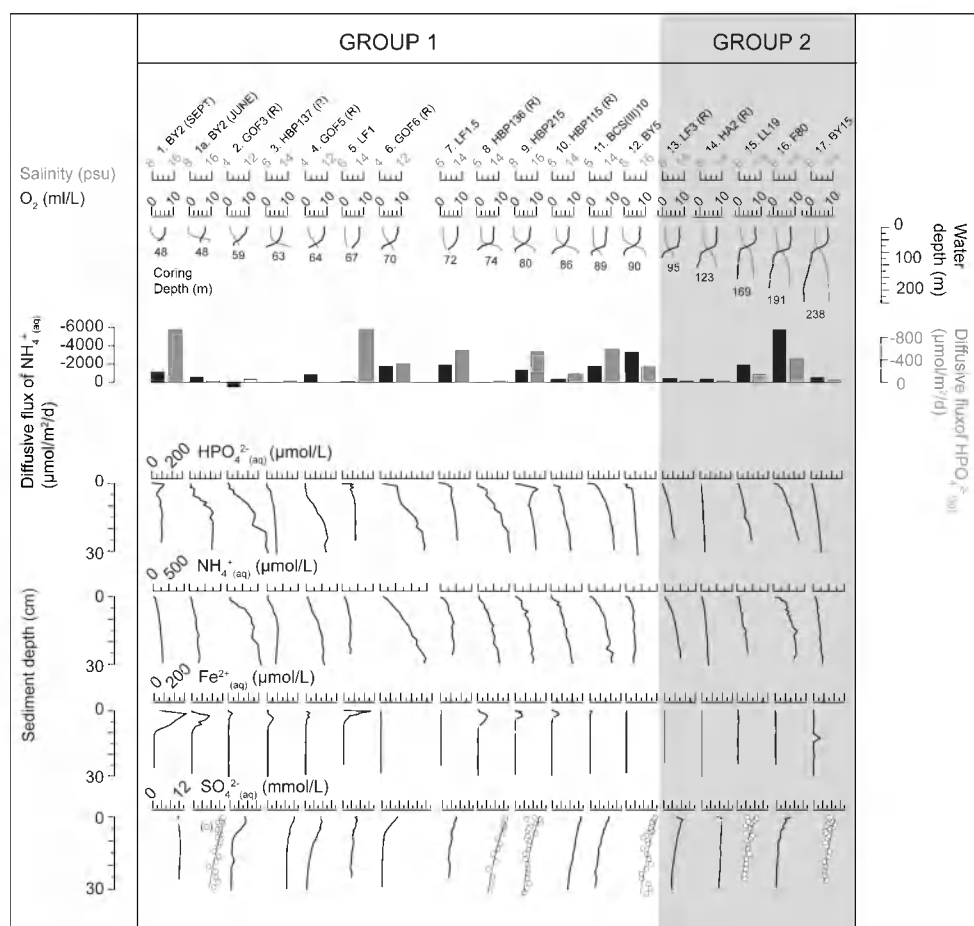
Fig. 2. Data array of sites used in this study, arranged by increasing water depth from left to right. Upper panel: Water column salinity and oxygen profiles. All profiles were measured during the HYPER/COMBINE cruise of the R/V *Aranda* in May/June 2009, except site 1. BY2 (Sept), for which profiles were measured during a cruise with the R/V Skagerak in September 2007 (Mort et al., 2010). Sub-zero oxygen concentrations are estimated from hydrogen sulfide concentrations using the ratio 1 mol H_2S = 2 mol O_2 (see Fonselius, 1981). Middle panel: Diffusive fluxes of NH_4^+ and HPO_4^- across the sediment-water interface, calculated from the concentration gradient between bottom water and the uppermost porewater sample (0–0.5 cm depth for cores sliced for porewater extraction by centrifugation, 0–1 cm depth for cores sample with rhizons, indicated "R") using Fick's first law:

$$F = -\frac{\varphi \cdot D}{\theta^2} \frac{\partial C}{\partial z}$$

where F = flux in $\mu mol\, m^{-2}\, day^{-1}$, and minus sign indicates an efflux from the sediments, D = ion-specific diffusion coefficient, corrected for temperature, taken from Boudreau (1997) and adjusted for salinity according to Van Cappellen and Wang (1995), ϕ = porosity and θ = tortuosity, defined as per Boudreau (1997):

$$\theta^2 = 1 - \ln\left(\varphi^2\right)$$

Lower panel: Porewater profiles of HPO_4^-, NH_4^+, Fe^{2+} and SO_4^{2-}. See text for details of sampling resolution and processing. SO_4^{2-} profiles for six sites are presented as logarithmic best-fit lines through raw data due to high scatter (data point in brackets for BY2 (June) not included in fit). All other profiles represent raw data only.

sediment-water interface was actively elevating the HPO_4^{2-} flux (relative to the expected flux from organic matter remineralization alone) at these sites at the time of sampling. Conversely, the lack of shallow-subsurface HPO_4^{2-} peaks at Group 2 sites suggests that iron oxyhydroxides are not presently involved in the P cycle at these water depths, and hence that organic matter remineralization alone dictates the rate of HPO_4^{2-} regeneration. Two Group 1 sites (BY2 and GOF5) record anomalously high NH_4^+/HPO_4^{2-} flux ratios of 19 and 83, respectively (Fig. 3a). The porewater HPO_4^{2-}
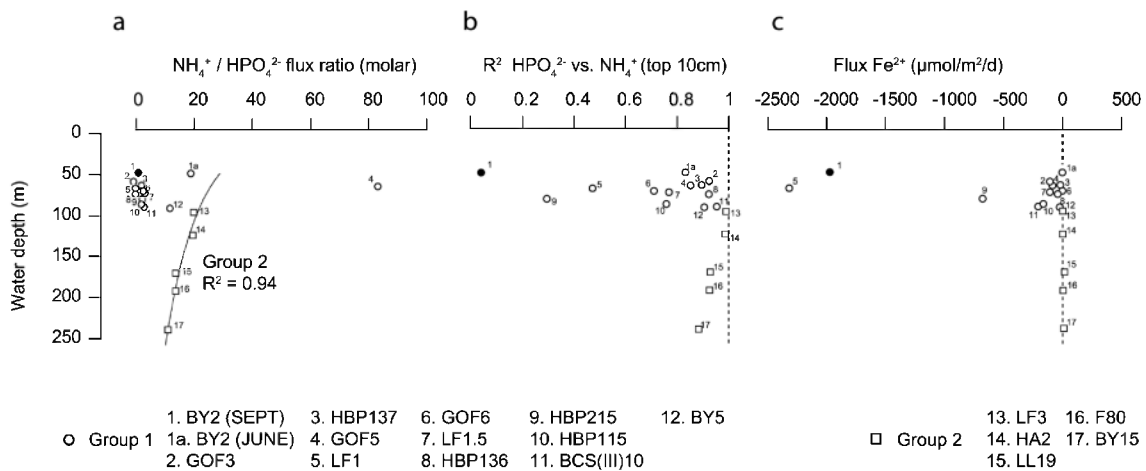
Fig. 3. **(a)** Ratio of diffusive fluxes of NH_4^+/HPO_4^- across the sediment-water interface vs. water depth for all sites. **(b)** Coefficient of determination (R^2) for linear regression between porewater profiles of NH_4^+ and HPO_4^- in the uppermost 10 cm of each core. Low R^2 indicates deviation of HPO_4^- profile from asymptotic shape, caused by dissolution of Fe-P in surface sediments. Vertical dashed line represents perfect correlation ($R^2 = 1$). **(c)** Diffusive flux of Fe^{2+} vs. water depth for all sites. Negative = efflux.
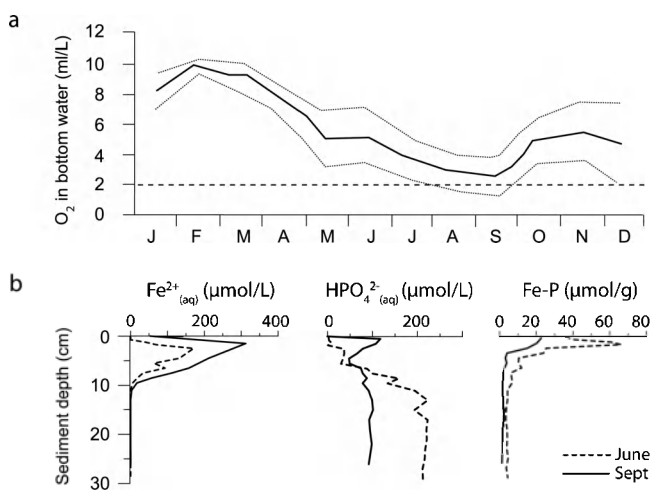

Fig. 4. **(a)** Seasonal variability in bottom water oxygen concentration at site BY2 in the Arkona Basin. Solid line represents mean values of 1995–2009, dotted lines the 20 % and 80 % quantiles. Data from Baltic Sea Environmental Database at Stockholm University, and Swedish Meteorological and Hydrological Institute. **(b)** Porewater profiles of HPO_4^- and Fe^{2+}, and solid phase profile of Fe-P at site BY2 in June and September sampling campaigns.

profiles at these sites display low values in the uppermost ∼5 cm, and an increase below this depth (Fig. 2). Such profiles are characteristic of sediments with an intact layer of iron oxyhydroxides at the sediment-water interface (Slomp et al., 1996; Slomp et al., 1998) which adsorb HPO_4^{2-}, thereby suppressing the diffusive flux of HPO_4^{2-} and elevating the NH_4^+/HPO_4^{2-} flux ratio.

The total hypoxic area in the Baltic varies annually by some $10\,000\,km^2$ (in a total of $20\,000\text{–}70\,000\,km^2$, depending on the position in the inflow-stagnation cycle (Conley et al., 2002), due to the annual cycle of organic matter loading to the sediment-water interface (Stigebrandt, 1991). A substantial area of sediments above and within the halocline thus experiences major variability in redox conditions throughout the year, which may be expected to influence the interaction between iron oxyhydroxides and HPO_4^{2-} regeneration (Reed et al., 2011). Closer inspection of the data from site BY2, sampled both in June 2009 and September 2007, confirms the strong influence of seasonal redox variability on the P cycle. In the season of greatest oxygen stress (represented by September 2007), porewater peaks of HPO_4^{2-} and Fe^{2+} are present close to the sediment-water interface (Fig. 4), driving high diffusive fluxes of both species and suppressing the NH_4^+/HPO_4^{2-} flux ratio (Figs. 2, 3). At this time, the concentration of Fe-P in the surface sediments is ∼20 µmol g^{-1} (Fig. 4). In contrast, during more oxic conditions (represented by June 2009) the subsurface porewater peaks of HPO_4^{2-} and $Fe^{2+}$are smaller and displaced downwards, enhancing the NH_4^+/HPO_4^{2-} flux ratio, while the surface sediments contain up to 40–60 µmol g^{-1} Fe-P (note: raw Fe-P data for BY2 in June 2009 are presented in Table B1). Furthermore, the mass of Fe-P in the upper 20 cm of a 1 cm^2 sediment column in September 2007 was 21.4 µmol, compared with 49.1 µmol June 2009 (calculated from the profiles in Fig. 4 and dry bulk density data, not shown). These results confirm that a substantial fraction of the pool of P associated with iron oxyhydroxides in surface sediments at BY2 (∼27.7 µmol cm^{-2}) may be quickly regenerated to the water column during seasonal outbreaks of hypoxia, and

conversely that P may be efficiently sequestered back to the sediments as oxygen conditions improve. It is noteworthy that seasonal outbreaks of even mildly "hypoxic" bottom water conditions, such as those observed at BY2 in September (Fig. 4), are able to trigger such a strong response in sedimentary Fe and P dynamics. Hence, although geochemical processes in bottom waters may not be expected to vary greatly across the biologically-defined "hypoxia" threshold of $2 \, \mathrm{ml} \, \mathrm{L}^{-1}$ dissolved oxygen, the vertical migration of redox zones within the underlying sediments leads to strong responses in sediment- and porewater-chemistry.

Due to the effects of seasonality, the data in Fig. 3 should be observed as a snapshot of conditions at the time of sampling. All sites currently experiencing seasonality in bottom water oxygen concentrations – hence all Group 1 sites – may reasonably be expected to show a variable flux of HPO_4^{2-} across the sediment-water interface throughout the year. The HPO_4^{2-} flux at such sites is strongly coupled to bottom water oxygen stress and the rate of iron oxyhydroxide dissolution in the sediments (Reed et al., 2011). The precise timing of the maximum HPO_4^{2-} flux may vary from site to site, due to the changing shape of the organic carbon loading curve in different regions of the Baltic (Stigebrandt, 1991), the ventilating action of small-scale inflows, and the water-depth dependent severity of oxygen depletion. A combination of these factors may account for the apparent offsets between the characteristics of BY2 and GOF5, versus the other Group 1 sites sampled in May/June 2009 (Fig. 3). In contrast, the Group 2 sites have experienced continuous hypoxia/anoxia throughout the year since early in the current stagnation, and the absence of iron oxyhydroxides in the surface sediments may be considered permanent within that time frame.

Closer inspection of the NH_4^+/HPO_4^{2-} flux ratios at the five Group 2 sites (Fig. 3a) shows a trend of decreasing values from ~ 20 at the shallowest of the sites (LF3, 95 m) to ~ 10 at the deepest (BY15, 238 m). This observation suggests that the remineralization rate of P relative to N from organic matter in the surface sediments increases with water depth, supporting the concept of accelerated regeneration of P from sediments with increasing severity of anoxic conditions (eg., Algeo and Ingall, 2007; Ingall et al., 1993; Kraal et al., 2010; Slomp et al., 2002). The mechanism of this process remains uncertain, but may be related to redox-dependent variability in the storage or release of P by sedimentary micro-organisms during the breakdown of organic matter (see discussion in Ingall and Jahnke (1997)).

3.2 Surface-sediment organic matter composition and relationship to regeneration fluxes

Surface sediment organic C:N:P ratios allow the hypothesis of accelerated remineralization of P with increasing water depth to be tested. Hypothetically, if organic matter arriving at the sediment-water interface at all sites had a consistent N:P ratio (Redfield or otherwise), surface sediment $N_{tot}:P_{org}$

should display the inverse trend to that of the NH_4^+/HPO_4^{2-} flux ratio; namely an increase with water depth, reflecting the increase in preferential remineralization of P. With some scatter, mean $N_{tot}:P_{org}$ in the top 2 cm of sediment at the ten sites selected for solid-phase analysis indeed shows an increase with water depth, from 32 at GOF3 to 57 at LL19 (Fig. 5a). The trend includes both Group 1 and Group 2 sites, suggesting that NH_4^+/HPO_4^{2-} flux ratios at Group 1 sites would likely show the inverse relationship if the Fe-P interaction was not active. A similar pattern is also observed in $C_{org}:P_{org}$, ranging from 328 at LF1 to 626 at LL19 (Fig. 5b), confirming that P is also preferentially remineralized relative to C with increasing oxygen stress (note that all raw C_{org}, P_{org} and N_{tot} data are presented in Table B1). The shape of the $N_{tot}:P_{org}$ and $C_{org}:P_{org}$ vs. water depth relationships most likely reflects the change in water column oxygen with depth, with a higher rate of change per vertical meter in the Group 1 sites where oxygen decreases rapidly close to the halocline. Although reported as C_{org}: total P (P_{tot}) and not explicitly stated by the authors, a depth-dependence in surface sediment C:P ratios is also seen in the data of Emeis et al. (2000), with highest values at three stations of >200 m depth in the Gotland Deep. Our maximum $C_{org}:P_{org}$ values of 500–650 indicate a ~ 5–6 fold sedimentary enrichment of C relative to P from the Redfield ratio of 106:1, which is comparable to the values in Mediterranean sapropels (300–1085, Kraal et al., 2010; Slomp et al., 2002), modern anoxic Black Sea sediments (mean value 558, Van Cappellen and Ingall, 1997) and Arabian Sea oxygen minimum zone sediments (400–800, Schenau and de Lange, 2001).

Interestingly, the convergence point of the exponential curves describing the NH_4^+/HPO_4^{2-} flux ratio and surface sediment $N_{tot}:P_{org}$ is close to N:P = 27 (Fig. 5a). One interpretation of this value is that it approximates the $N_{tot}:P_{org}$ ratio of organic matter arriving at the sediment-water interface, and that during subsequent organic matter degradation, the NH_4^+/HPO_4^{2-} flux ratio and $N_{tot}:P_{org}$ in the upper 2 cm of sediment then diverge to lower and higher values, respectively. The extent of the divergence is controlled by redox conditions in the sediments, with strongly reducing conditions causing the greatest offset. The initial value of 27 represents a two-fold enrichment relative to Redfield stoichiometry and appears high compared to the mean N:P values of material caught in sediment traps in the Gotland Deep (~ 9–11, Emeis et al., 2000; Struck et al., 2004). However, these studies report $N_{tot}:P_{tot}$, which may be suppressed by sinking or suspended non-organic P phases such as Fe-P and detrital-P. Dellwig et al. (2010) show maxima in suspended MnO_x-$FeOOH$-PO_4 in the vicinity of the redoxcline in the Gotland Deep, and in suspended $FeOOH$-PO_4 over a broad (at least 40 m) depth range immediately below the redoxcline. Thus, both the 140 m and 230 m traps reported in Emeis et al. (2000) could potentially have collected non-organic P from these suspended phases, influencing the $N_{tot}:P_{tot}$ ratios. The convergence point in our sediment and diffusive
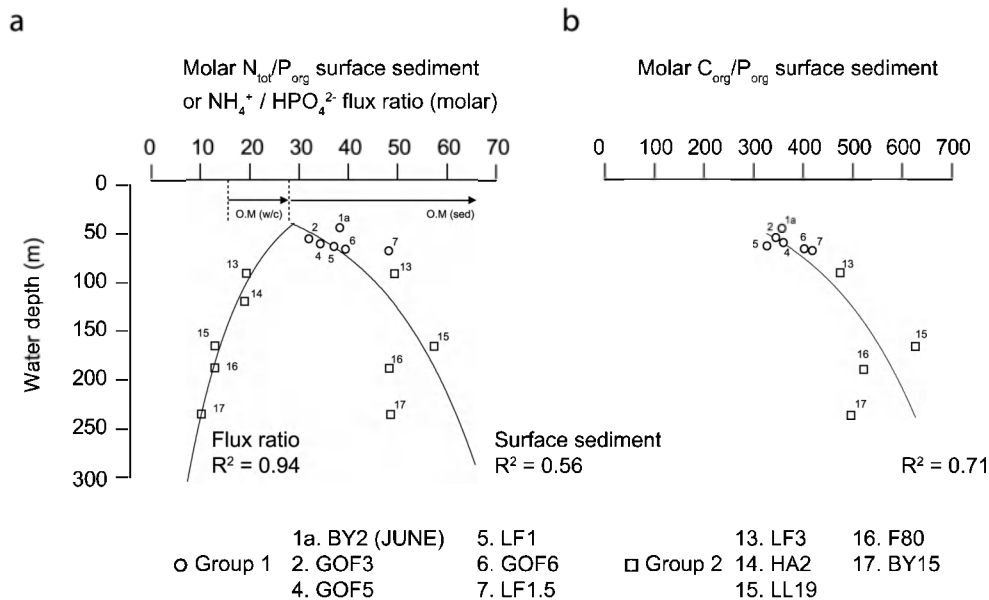
Fig. 5. (a) NH_4^+/HPO_4^- diffusive flux ratio at all Group 2 sites (left trendline and data), and sedimentary N_{tot}/P_{org} ratio in the upper 2 cm of sediment at sites selected for solid phase analyses (from both Group 1 and 2, right trendline and data), plotted against water depth. Vertical dashed lines indicate Redfield ratio (N:P = 16) and the intersection of the two trendlines (N:P = 27). Arrows represent inferred progression of N:P ratio of organic matter during descent through the water column ("OM (w/c)"), from 16 → 27, and in the surface sediments (OM (sed)), from 27 → a higher value, whose magnitude is determined by water depth-dependent preferential remineralization of P. **(b)** Sedimentary C_{org}/P_{org} ratio in the upper 2 cm of sediment at the same sites plotted for N_{tot}/P_{org} in **(a)**.

flux data therefore provides a useful alternative estimate of the change in the N:P ratio of organic matter from its initial Redfield proportions during degradation in the water column, i.e. 16 → 27 (Fig. 5a). At Group 1 sites, this may surpass the magnitude of the change which subsequently occurs during degradation in the sediments (27 → 32 − 48), whereas for Group 2 sites the change after deposition (27 → 48 − 57) is greater than that in the water column. Lateral transport of organic material across the seafloor (Emeis et al., 2002; Jonsson et al., 1990) may allow older, partially degraded organic material to accumulate at deeper sites, potentially influencing the measured surface sediment $N_{tot}:P_{org}$. Specifically, organic material experiencing degradation during downslope transport – thus in relatively oxic conditions compared to those in the deep basin accumulation zone – would be expected to acquire depleted $N_{tot}:P_{org}$ and $C_{org}:P_{org}$ ratios, and therefore to dilute deep-basin surface sediment $N_{tot}:P_{org}$ towards lower values. This phenomenon could account for part of the scatter in the sediment data of Fig. 5a, most notably the relatively depleted $N_{tot}:P_{org}$ and $C_{org}:P_{org}$ ratios at F80 and BY15. However, the lack of such scatter in the NH_4^+/HPO_4^{2-} flux ratio ($R^2 = 0.94$ for all Group 2 sites) suggests that the laterally transported material is refractory once accumulated in the deep basins and does not contribute significantly to remineralization at these depths.

3.3 Implications of preferential P remineralization for basin-scale DIP during inflow-stagnation cycles

Due to preferential remineralization of P, Redfield-based modeling of organic matter breakdown in the Baltic may underestimate the magnitude of the direct remineralization flux to the total rate of P regeneration during stagnations, and hence the total pool of P in the water column. Simple budget calculations based on the modeled deep-basin carbon and phosphorus flows of Gustafsson and Stigebrandt (2007) support this claim (Table 1). The model of Gustafsson and Stigebrandt (2007) calculates a mean burial efficiency of 48 % of all C_{org} passing through the 150 m water depth horizon in the Gotland Deep. Using this value, and measured deep-basin C_{org} and P_{org} accumulation rates (from this study, Hille, 2005 and Hille et al., 2005), it can be shown that preferential remineralization of P from the buried fraction (48 %) of the organic matter adds 0.13–0.29 g m^2 yr^{-1} P to the 0.32–0.39 g m^2 yr^{-1} P released during complete remineralization of the other 52 %. This is of a similar order of magnitude to the mean value of R_{Fe} – the "additional" amount of P required to balance observed water-column concentrations – during five completely anoxic stagnations since 1965 in the Gotland Deep (Gustafsson and Stigebrandt, 2007). R_{Fe} is assumed to represent the dissolution of sedimentary Fe-P, thus the non-zero values during completely anoxic stagnations are unexpected, since no iron oxyhydroxides should be present

Table 1. Summary of carbon and phosphorus fluxes in deep basins of the Baltic.

		A	B	C	D	E	F	G	H
Parameter		C_{org} accumulation rate in sediments	Flux of C_{org} through 150 m depth horizon*	Rate of complete remineral-ization of C_{org}	Rate of complete remineral-ization of P_{org}	Remaining P_{org} available for burial	P_{org} accumulation rate in sediments	Preferential remin. flux of HPO_4^{2-} into water column	Mean excess HPO_4^{2-} flux during anoxic stagnations*
Calculation		Measured	$2.07 \times A$	B–A	$C/41$ $(g\,m^{-2}\,yr^{-1})$ $C/106$ $(\mu mol\,m^{-2}\,d^{-1})$	$A/41$ $(g\,m^{-2}\,yr^{-1})$ $A/106$ $(\mu mol\,m^{-2}\,d^{-1})$	Measured	E–F	
Code (Gustafsson and Stigebrandt, 2007)		$(F_{SA})_{Corg}$	$(F_O)_{Corg}$	$(R_O + R_{DEN})_{Corg}$					R_{Fe}
Coring site (study)									
	$g\,m^{-2}\,yr^{-1}$								
F80, Fårö Deep, 0–5 cm of sediment= 2003–present (this study)		12.2	25.2	13.0	0.32	0.30	0.17	0.13	0.30
Mean of 53 cores in Gotland basin (Hille 2005; Hille et al., 2005)		14.8	30.6	15.8	0.39	0.36	0.07**	0.29	0.30
	$\mu mol\,m^{-2}\,d^{-1}$								
F80, 0–5 cm= 2003–present (this study)		2785	5759	2974	28	26	15	11	27
Mean of 53 cores in Gotland basin (Hille 2005; Hille et al., 2005)		3379	6986	3607	34	32	6	26	27

* Calculated from fluxes in budget of Gustafsson and Stigebrandt et al. (2007).
** Estimated from total P accumulation rates of Hille et al. (2005) and mean P_{org}: total P ratio of top 2 cm of F80, BY15 and LL19 (0.36, Table B1).

in the surface sediments in such intervals. Lateral transport of sedimentary material downslope into the deep basins of the Baltic (e.g., Emeis et al., 2002) may potentially contribute P via dissolution of Fe-P transported across the redoxcline. While this flux remains poorly quantified, our calculated magnitude of the preferential remineralization flux is sufficient to explain 0.13–$0.29\,g\,m^2\,yr^{-1}$ of the $0.30\,g\,m^2\,yr^{-1}$ "additional" P (R_{Fe}) observed during anoxic stagnations (Table 1). Considering the uncertainties involved, we may conclude that preferential remineralization accounts for a major proportion of R_{Fe} during anoxic stagnations, with an additional contribution most likely derived from dissolution of laterally-transported Fe-P. These factors can also explain the scatter in the "R_{Fe} vs. anoxic bottom increase" trend during variable redox stagnations (Fig. 10 in Gustafsson and Stigebrandt 2007).

In light of the proposed mechanisms for accelerated accumulation of HPO_4^{2-} in the deep waters, the relationship between total hypoxic area (A) and the total water column pool of HPO_4^{2-} (DIP) proposed by Conley et al. (2002) may be re-examined. Although the period 1970–2000 investigated by these authors encompasses several shorter multi-

annual inflow-stagnation cycles, a clear secular trend is observed of contraction in the total hypoxic area from 1970–1993, followed by an expansion from 1994–2000, with the major inflow of 1993 acting as the switching point (Fig. 6a and Conley et al., 2002). The extended dataset of 1962–2006 presented in Conley et al. (2009a) confirms that this pattern forms part of a multidecadal oscillation in hypoxic area in the Baltic since the middle of the 20th century. Conley et al. (2002) showed that the net annual change in A (ΔA) and ΔDIP are positively correlated in the 1970–2000 dataset, due to net uptake or release of P by sedimentary iron oxyhydroxides from one year to the next. However, the relationship between the raw values of A and DIP for the full 1970–2000 dataset is less conclusive (Fig. 6b), implying that the Fe-P interaction cannot fully explain the secular trends in DIP. When the data is divided into the intervals 1970–1993 and 1994–2000, it becomes clear that while the relationship between A and DIP during the expansion phase (1993–2000) is indeed strongly positive, during the contraction phase (1970–1993) the relationship is weakly negative (Fig. 6b). The switchbacks in the time series of the contraction phase contribute to the weakness of the correlation, and
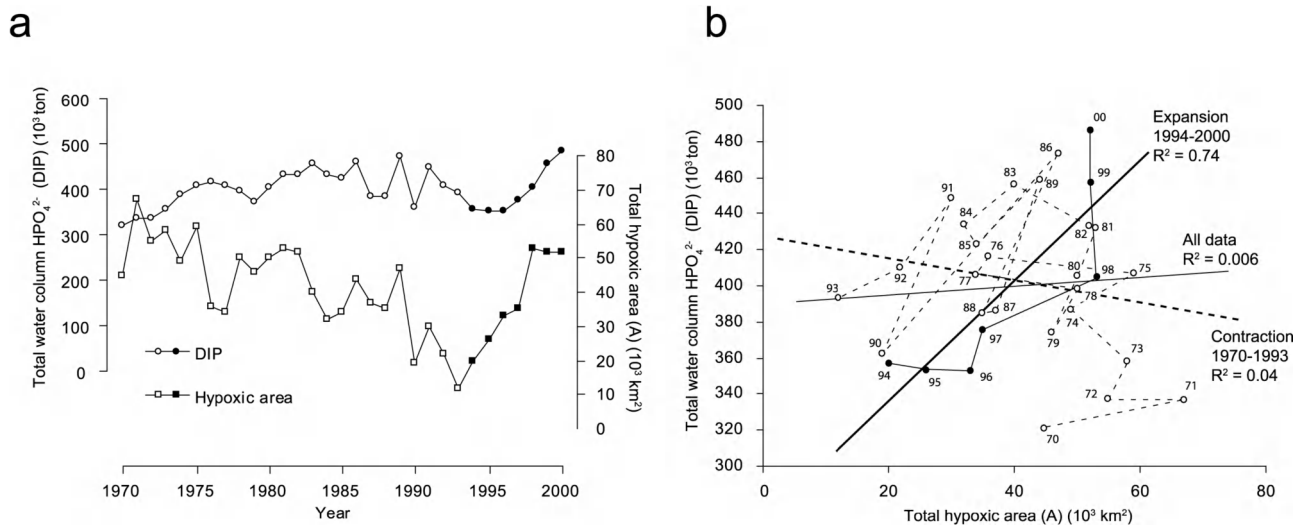
a

b

Fig. 6. (a) Time series of total hypoxic area of the Baltic ("A", square symbols), i.e. the area of sediments in contact with bottom waters of <2 ml L^{-1} O_2, and the total pool of dissolved inorganic phosphate (DIP, circles). Both series averaged for January-March for each year from 1970-2000 (data from Table 1 in Conley et al., 2002). Open symbols indicate 1970-1993 "contraction" of hypoxic area, closed symbols represent 1994-2000 "expansion" phase. **(b)** Cross-plot of the same data. Trend for complete dataset shown as a fine solid line. Data points for 1970-1993 (open circles) are joined chronologically with a dashed line. Note the frequently positive relationship between annual changes in A and DIP but the overall negative trend for this interval (dashed trendline). Data points for 1994-2000 (filled circles) are joined chronologically with a solid line (heavy solid trendline represents 1994-2000 trend).

confirm the generally positive relationship between ΔA and ΔDIP identified by Conley et al. (2002), with 15 of the 22 annual steps displaying a positive gradient. However, the results clearly indicate that during contraction of the hypoxic area on the multidecadal timescale from 1970-1993, a net trend towards higher DIP is observed, despite the ongoing uptake of P by iron oxyhydroxides as a larger area of surface sediments becomes oxic. This observation implies that during the contraction phase, release of HPO_4^{2-} into the water column below the halocline, via direct remineralization from organic matter in the surface sediments and in the water column itself, on balance outweighs the uptake of P by iron oxyhydroxides at shallower depths. Simply stated, although the volume of hypoxic water shrinks, the total mass of HPO_4^{2-} in the water column increases. Both preferential remineralization of P from organic matter and dissolution of Fe-P transported laterally into the deep basins may contribute to accelerated accumulation of HPO_4^{2-}. In contrast, the strong positive correlation between A and DIP in the expansion phase of 1994-2000 can be explained by the fact that both organic matter remineralization and the dissolution of surface-sediment iron oxyhydroxides along the basin margins act in unison to release HPO_4^{2-} into the water column as the hypoxic area expands.

3.4 Temporal variability in P burial with expansion and contraction of hypoxic area

The strong multidecadal oscillations in total hypoxic area may be expected to influence spatial patterns not only of P regeneration, but also of P burial, especially around the margins of the deep basins where redox conditions are most variable. Mort et al. (2010) showed that organic P (P_{org}) is the dominant burial phase of reactive (non-detrital) P throughout most of the modern Baltic, due to the poor preservation of Fe-P below the sediment surface and the lack of authigenic Ca-P formation within the upper 30 to 50 cm of the sediment column. To investigate the recent evolution of P_{org} burial in response to changes in hypoxia, we focus on dated sediment records from three sites (LF1, LF1.5 and LF3, Fig. 1) along a depth transect into the Fårö Deep in the central Baltic (details of the ^{210}Pb age models are presented in Table C1). A long archive of water column monitoring data is available for comparison from site F80 in the central Fårö Deep, allowing reconstructions of water column oxygen conditions from 1910 onwards. Conditions in the central basin do not translate directly to those at equivalent depth along the basin margins, as shoaling of the halo/redoxcline in shallower waters dictates an offset towards lower oxygen concentrations at the shallower sites (see Fig. 16 in Al-Hamdani and Reker, 2007). However, the multidecadal trends in oxygen concentration in the 70-90 m depth range are expected to be qualitatively similar throughout the basin, making such a comparison valid.

Water column oxygen concentrations at 70–90 m in the Fårö Deep declined from 1910–1970, crossing the threshold into hypoxia $(2\,\mathrm{ml\,L^{-1}})$ in the lower part of the depth range. From 1970–1993, during contraction of the hypoxic area (and thus deepening of the water column redoxcline), oxygen concentrations increased, before declining again during expansion of the hypoxic area from 1994–2000. The accumulation rates of P_{org} at LF1, LF1.5 and LF3 show a clear inverse co-variation with oxygen concentrations throughout the 20th century, with maxima close to 1970 and minima close to 1992, confirming the observations of Mort et al. (2010) that P_{org} accumulation in Baltic Sea sediments increases with hypoxia. Although organic matter degradation within the upper sediments is expected to remove a portion of accumulated P_{org} prior to permanent burial, reactive transport modeling of organic matter degradation at these sites (unpublished results) suggest the influence of such breakdown at the current depth of the 1970–2000 interval is negligible, hence accumulation may be considered equivalent to burial. Furthermore, the accumulation rate of C_{org}, and sedimentary C_{org}:P_{org} ratios, show a roughly parallel evolution to that of P_{org} accumulation. This indicates that although enhanced preferential P remineralization occurred at these sites during intervals of lower oxygen concentrations (thus maximum hypoxic area), net P_{org} burial nevertheless increased due to enhanced burial of its host phase, organic matter.

The effects of the multidecadal expansion and contraction of the hypoxic area on P regeneration and burial are summarized in Fig. 8, in which the Fårö Deep is shown as representative for the deeper sections of the Baltic Proper. During intervals of maximum hypoxic area such as the early 1970s, the halocline and redoxcline were comparatively shallow, with hypoxia occurring below ~70 m water depth in the central part of the basin. The zone of sediments along the basin margins containing Fe-P was therefore comparatively small, and LF1, LF1.5 and LF3 were all situated below the redoxcline. Hence, LF1, LF1.5 and LF3 in the early 1970s would qualify as Group 2 sites, characterized by the absence of Fe-P at the sediment surface, a high net rate of P_{org} burial, and enhanced preferential remineralization of P relative to C. Conversely by 1992, the halocline and redoxcline were displaced much deeper in the water column, qualifying LF1, LF1.5 and LF3 as Group 1 sites with Fe-P seasonally present in the surface sediments, a comparatively low net rate of P_{org} burial, and limited preferential remineralization of P relative to C. However, despite the deeper redoxcline, the long stagnation of the bottom waters in the years leading up to 1992 generated a comparatively large total pool of water column DIP in the deepest part of the basin.

3.5 Wider implications for P-driven eutrophication/hypoxia feedbacks and basin-scale biogeochemical modeling

Preferential remineralization of P from organic matter in the water column and sediments, and the consequent accumulation of HPO_4^{2-} below the halocline, clearly exert a strong control on the basinwide pool of DIP in the Baltic. However, since the total DIP pool largely consists of DIP stored in the deep waters, there remains much debate over its influence on P availability in the photic zone, and hence the efficiency of the positive feedback between P regeneration, eutrophication and sustained hypoxia. Upwards transport of HPO_4^{2-} across the halocline is predicted by the principles of turbulent diffusion (Gustafsson and Stigebrandt, 2007) and has been calculated to account for 60 % of the annual replenishment of HPO_4^{2-} to surface waters (Vahtera et al., 2007). However, recent evidence suggests that up to 40–60 % of the flux estimated from the $[HPO_4^{2-}]$ gradient may in fact be trapped and recycled by particulate iron and manganese oxyhydroxides in the water column (Turnewitsch and Pohl, 2010). This process may contribute to the low correlation observed between winter HPO_4^{2-} concentrations above and below the halocline at sites in the open Baltic (Lilover and Stips, 2008). Furthermore, the physical mechanisms determining P transport to the surface, ie. wind-driven mixing in winter (Janssen et al., 2004) and summer upwelling along coastal margins (Nausch et al., 2009) are sensitive to climatic parameters and thus vary on multiannual to multidecadal timescales.

Changes in the spatial distribution of the deep-water DIP pool (Fig. 8) may influence its accessibility to vertical transport processes such as mixing and upwelling, and thus may be equally as important as the size of the pool itself in determining the total rate of P supply to the surface waters. A major challenge for future biogeochemical modeling of the Baltic is thus to unravel how the two contrasting – and naturally forced – states presented in Fig. 8 differ in their capability to sustain eutrophication and hypoxia. Especially with regards to the planning of hypoxia remediation strategies (Conley et al., 2009b), knowledge of the expected response of the system to changes in total hypoxic area is crucial. The enhanced C_{org} burial observed along the deep basin margins during intervals of maximum hypoxic area (Figs. 7, 8) is likely a combined signal, both of deteriorating redox conditions and of higher export productivity, analogous to the mechanisms by which Mediterranean sapropel sediments are formed (e.g., de Lange et al., 2008). If so, intervals of maximum hypoxic area such as the early 1970s may well be characterized by a more efficient P regeneration-eutrophication-hypoxia feedback loop than intervals of minimum hypoxic area, with all fluxes in the P cycle accelerating despite the smaller total DIP pool in the water column. This would imply that the accessibility of the DIP pool (which is greater due to its shoaling during intervals of maximum hypoxic area)
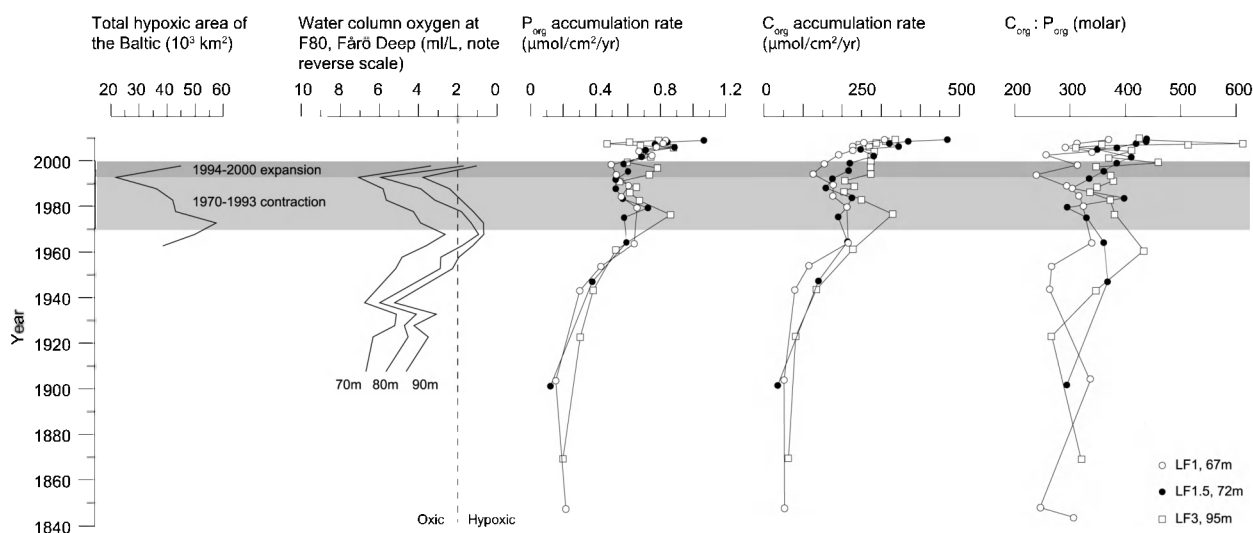
Fig. 7. Time series of C_{org} and P_{org} accumulation rates, and C_{org}/P_{org}, at sites LF1, LF1.5 and LF3 on the margins of the Fårö Deep in the central Baltic, and relevant water column oxygen data. C_{org} and P_{org} accumulation rates were calculated from ^{210}Pb-derived mass accumulation rates (estimated using a Constant Rate of ^{210}Pb Supply (CRS) model (Boer et al., 2006) and C_{org} and P_{org} contents). Total hypoxic area data from Conley et al. (2009) and water column oxygen concentrations at site F80 from the Baltic Sea Environmental Database at Stockholm University are plotted as 5 year binned mean values.

indeed outweighs the size of the pool in determining the net upwards flux of P to the surface waters.

4 Conclusions

A comprehensive coring survey has facilitated an unprecedented investigation of the controls on regeneration and burial of P throughout the Baltic Sea. The network of pore-water data provide a snapshot of conditions during the current stagnation interval (2003-present), and reveal a strong depth-dependence of the processes controlling regeneration of P from the sediments. Sites of ≤ 90 m water depth currently display evidence for the interaction between P and iron oxyhydroxides in the surface sediments, confirming the earlier work of Mort et al. (2010). Seasonal variability in bottom-water redox conditions at such sites results in a strong annual cycle in the efflux of P, with maximum release during the most reducing months when iron oxyhydroxides reductively dissolve. In contrast, sites below 90 m display a continuous efflux of P, reflecting degradation of sedimentary organic matter. Moreover, the rate of P regeneration (relative to C and N) from degrading organic matter is controlled by the ambient redox conditions, and hence is itself depth-dependent, with maximum preferential P remineralization occurring in the deep basins. Such preferential P remineralization leads to depletion of the diffusive flux ratio of NH_4^+/HPO_4^{2-}, and enrichment of sedimentary $N_{tot}:P_{org}$ and $C_{org}:P_{org}$, with increasing water depth. The data suggest a roughly two-fold enrichment of the $N_{tot}:P_{org}$ ratio of organic matter from its original Redfield proportions during

descent through the water column, followed by further enrichment after accumulation at the sediment-water interface. These processes lead to a substantial build-up of excess P in the water column, which is underestimated by existing Redfield-based modeling of biogeochemical cycles during previous stagnation intervals. Furthermore, the magnitude of preferential remineralization of P in the deep basins was great enough to generate a net increase in the total water column pool of DIP during contraction of the hypoxic area from 1970–1993, despite the large scale sequestration of P into iron oxyhydroxides at shallower depths during this time.

Burial of reactive P in the Baltic takes place principally as organic P, and the rate of organic P burial along the margins of the deep basins is redox dependent, with higher burial during intervals of more reducing conditions. Expansion of the total hypoxic area on the multidecadal timescale thus leads to expansion of the area of enhanced burial of organic P, despite a simultaneous increase in the rate of preferential remineralization of P from organic matter and the large-scale dissolution of P associated with iron oxyhydroxides. This may imply an accelerated P cycle during intervals of maximum hypoxic area, in which the rates of P incorporation into organic matter, regeneration from and burial within the sediments are all enhanced. Such a scenario may be supported physically by efficient upwards transport of deep water HPO_4^{2-} across the shallow halocline present during these intervals.
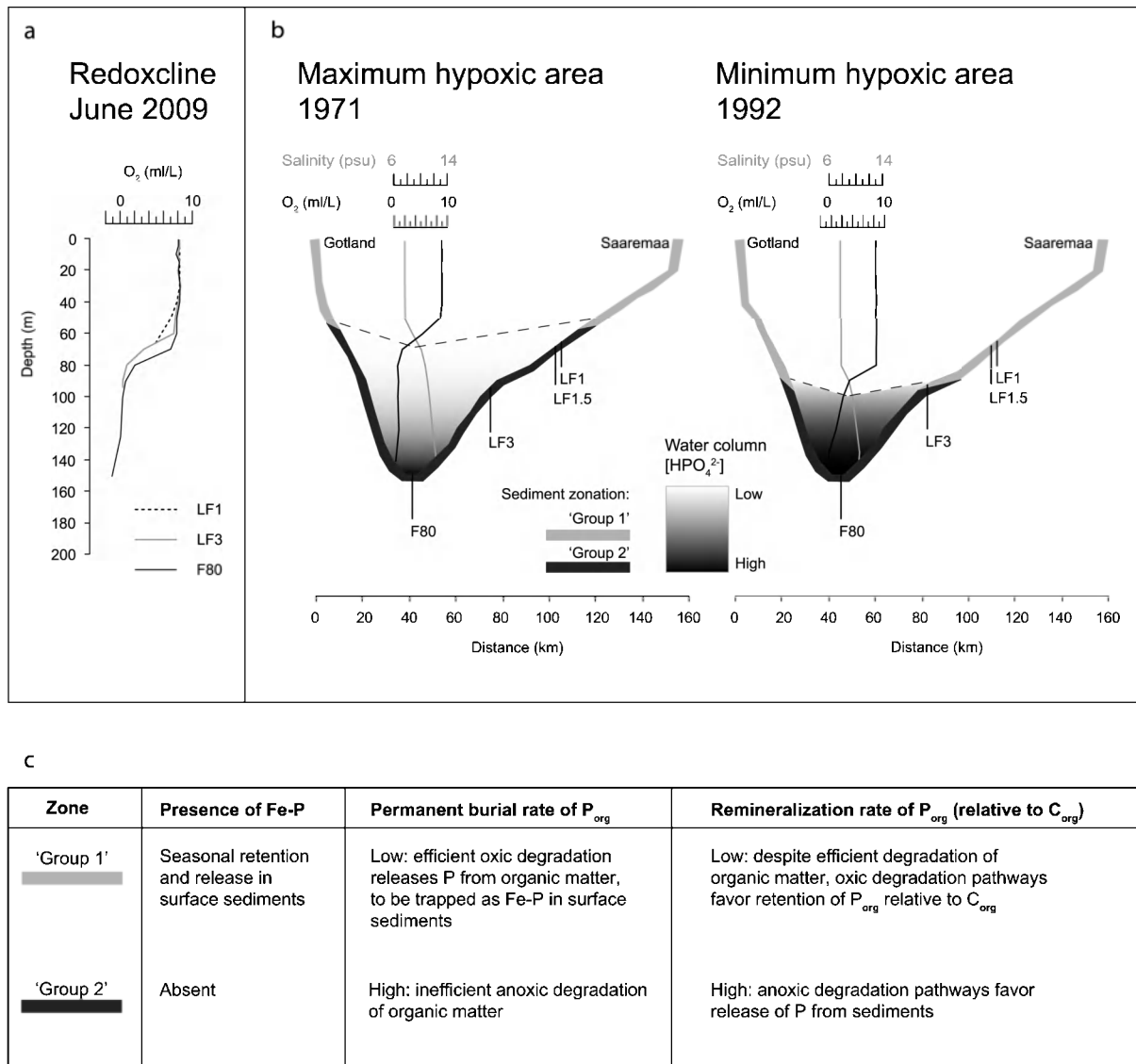
Fig. 8. (a) Water column oxygen concentrations measured during the R/V *Aranda* cruise of May/June 2009 at sites LF1, LF3 and F80 along a depth transect into the Fårö Deep between the islands of Gotland and Saaremaa, showing the vertical offset of the redoxcline between central (F80) and marginal (LF1) sites. **(b)** Scaled cross-sectional sketches through Fårö Deep in 1971 and 1992 (simplified bathymetry from Data Assimilation System of Baltic Environmental Database, Stockholm University, depth scale as for **(a)**), showing water column salinity and oxygen profiles from F80 (also known as BY20, data from Baltic Environmental Database) in the month of February (chosen for comparable data availability). With the exception of F80, sites are positioned accurately by depth. The simplified bathymetry aliases the true depth of F80 (191 m, Fig. 2) and generates minor lateral offsets from true position of all sites. Dashed lines show approximate position of hypoxia threshold ($O_2 = 2 \, \text{ml} \, L^{-1}$) based on profiles at F80 and assumption of 15 m vertical offset of redoxcline between F80 and LF1 (see **(a)**). Shading in water column below halo/redoxcline qualitatively represents deep water [HPO_4^{2-}]. Sediment zones are divided based on the assumption that iron oxyhydroxides are absent from surface sediments below a threshold of oxygen stress which may be spatially variable but generally deeper than that of bottom water hypoxia. **(c)** Table summarizing characteristics of sediment zones with respect to the phosphorus cycle.

Table A1. Concentrations of porewater species in $\mu mol\,L^{-1}$ (R = sampled with rhizons) and bottom water oxygen concentrations in $ml\,L^{-1}$. Sub-zero oxygen concentrations are estimated from hydrogen sulfide concentrations using the ratio $1\,mol\,H_2S = 2\,mol\,O_2$ (see Fonselius, 1981).

Core	Sample mid-depth (cm, 0 = bottom water)	NH_4	SO_4	HPO_4	Fe
LF1					
Bottom water	0	50	6283	2	0
$O_2 = 4.77\,ml\,L^{-1}$	0.25	53	5535	106	257
	0.75	76	6276	84	209
	1.25	91	6347	79	143
	1.75	108	6362	108	140
	2.5	119	5952	78	53
	3.5	144	6005	95	44
	4.5	165	5649	97	20
	5.5	167	4869	109	4
	6.5	186	4901	115	0
	7.5	187	4516	119	0
	8.5	229	4206	121	0
	9.5	236	4772	125	0
	11	252	4830	126	0
	13	235	4411	125	0
	15	244	4017	127	0
	17	250	3890	129	0
	19	246	3831	128	0
	21	195	3329	127	0
	23	260	4086	128	0
	25	239	3930	128	0
LF1.5					
Bottom water	0	19	6312	2	0
$O_2 = 3.83\,ml\,L^{-1}$	0.25	77	6220	51	9
	0.75	123	6287	84	6
	1.25	147	5727	92	9
	1.75	187	5864	112	1
	2.5	217	5167	124	1
	3.5	252	5340	120	0
	4.5	270	5057	117	0
	5.5	260	4162	116	0
	6.5	297	4286	119	1
	7.5	340	3816	125	0
	8.5	377	4370	128	0
	9.5	397	4083	134	0
	11	436	3866	144	0
	13	373	3042	151	0
	15	396	3018	158	0
	17	377	2572	162	0
	19	429	3173	165	0
	21	444	3258	171	0
	23	432	3130	171	0
	25	393	2797	174	2
BCS(III)10					
Bottom water	0	42	8050	3	0
$O_2 = 1.19\,ml\,L^{-1}$	0.25	101	8371	58	19
	0.75	138	8196	76	9
	1.25	170	8226	84	0
	1.75	205	7827	94	0
	2.5	228	7238	109	0
	3.5	287	6895	117	0
	4.5	343	6624	130	0
	5.5	362	5721	139	0
	6.5	391	5966	152	0
	7.5	446	5405	164	0
	8.5	468	5024	176	0
	9.5	503	4881	179	0
	11	526	4766	193	0
	13	527	3569	207	0
	15	569	3676	217	0
	17	585	3266	219	0
	19	651	3109	236	0
	21	657	2661	240	0
	23	550	1906	248	0
	25	759	2575	245	0
	27	704	2444	251	0
	29	717	1929	254	0
BY5					
Bottom water	0	6	13310	2	0
$O_2 = 0.09\,ml\,L^{-1}$	0.25	108	13700	26	2
	0.75	90	12614	18	0
	1.25	106	12907	18	0
	1.75	148	12443	65	0
	2.5	167	12017	75	0
	3.5	200	12004	79	0
	4.5	217	11440	84	0
	5.5	247	11885	83	0
	6.5	229	10340	86	0
	7.5	221	9607	92	0
	8.5	218	8221	92	0
	9.5	252	9650	95	0
	11	272	10189	96	0
	13	239	7865	102	0
	15	274	9373	103	0
	17	280	10283	106	0
	19	293	11221	108	0
	21	283	9407	111	0
	23	235	7449	117	0
	25	239	7090	121	0
	27	285	10144	122	0
	29	293	11026	126	0
	31	296	9504	127	0
	33	294	8078	130	0
	35	295	8571	132	0

Table A1. Continued.

Core	Sample mid-depth (cm, 0 = bottom water)	NH$_4$	SO$_4$	HPO$_4$	Fe	Core	Sample mid-depth (cm, 0 = bottom water)	NH$_4$	SO$_4$	HPO$_4$	Fe
BY2							37	482	4128	223	2
Bottom water	0						39	590	4241	222	3
O$_2$ = 5.17 ml L^{-1}	0.25	15	13343	3	0		41	677	5114	227	1
	0.75	22	12610	4	0		43	697	5621	229	2
	1.25	33	12522	9	41	BY15					
	1.75	54	13300	1	70	Bottom water	0	33	7713	7	2
	2.5	57	10798	37	171	O$_2$ = −3.32 ml L^{-1}	0.25	47	7053	10	1
	3.5	79	11550	37	151		0.75	53	7497	12	2
	4.5	72	6608	35	133		1.25	74	8444	15	3
	5.5	116	10949	30	64		1.75	83	8386	18	3
	6.5	135	12098	88	93		2.25	93	8106	20	4
	7.5	134	12255	100	34		2.75	93	6896	23	6
	8.5	158	10958	158	18		3.25	117	9541	25	6
	9.5	190	12077	133	6		3.75	93	5865	27	4
	11	196	12059	194	0		4.25	122	8895	30	7
	13	195	10980	222	0		5	124	7740	33	4
	15	226	9256	193	0		6	106	5199	36	4
	17	278	11434	222	0		7	117	5734	39	6
	19	241	9822	219	0		8	156	7102	43	3
	21	243	7002	220	0		9	149	5804	47	3
	23	266	9851	216	0		10.5	142	5143	51	3
	25	297	10427	216	0		12.5	179	5935	58	68
	27	315	11346	211	0		14.5	193	7046	66	3
	29	276	9212	211	0		16.5	211	6557	71	3
HBP215							18.5	187	4835	76	3
Bottom water	0	12	8414	6	0		20.5	227	5257	81	11
O$_2$ = 0.26 ml L^{-1}	0.25	51	4722	52	58		22.5	219	4887	84	3
	0.75	113	10938	96	38		24.5	227	4849	89	1
	1.25	137	11349	146	62		26.5	272	6282	93	2
	1.75	200	11362	193	63		29.5	272	5707	96	2
	2.5	210	9316	224	68		33	254	4922	102	3
	3.5	198	6625	184	18		35	346	6435	94	4
	4.5	224	5836	173	2		36	336	6408	108	2
	5.5	246	5247	159	0		37	322	5360	105	4
	6.5	408	8788	152	0		38	359	6396	105	6
	7.5	314	5421	148	0		39	329	6333	110	7
	8.5	338	4993	146	0	F80					
	9.5	406	6124	135	16	Bottom water	0	66	6495	13	1
	11	444	5932	155	0	O$_2$ = −2.04 ml L^{-1}	0.25	207	6271	42	1
	13	483	5987	160	0		0.75	224	4292	52	1
	15	438	4379	171	0		1.25	253	4593	58	1
	17	493	4313	179	0		1.75	356	4763	75	1
	19	514	5296	186	0		2.5	405	4105	87	1
	21	523	5303	194	0		3.5	426	3261	97	2
	23	581	5300	200	3		4.5	467	3603	103	3
	25	521	5093	200	2		5.5	395	2363	114	2
	27	607	6003	205	2		6.5	503	2186	125	2
	29	569	4811	208	2		7.5	446	1941	127	3
	31	530	3585	211	3		8.5	546	2236	133	6
	33	554	4070	215	1		9.5	522	1415	148	7
	35	584	4907	219	2						

Table A1. Continued.

Core	Sample mid-depth (cm, 0 = bottom water)	NH$_4$	SO$_4$	HPO$_4$	Fe
	11	592	1010	166	3
	13	623	975	173	2
	15	769	1162	183	3
	17	661	635	199	3
	19	707	618	210	2
	21	721	347	221	2
	23	728	296	232	4
	25	744	312	247	3
	27	667	197	258	1
	29	710	56	271	1
	32	930	47	285	1
LL19 Bottom water O$_2$ = −0.89 ml L^{-1}	0	15	4944	4	3
	0.25	62	8891	14	2
	0.75	80	7967	19	3
	1.25	92	7966	22	4
	1.75	84	5166	21	4
	2.5	94	6723	32	8
	3.5	107	4233	35	9
	4.5	128	6007	41	9
	5.5	134	5339	47	13
	6.5	126	4048	51	7
	7.5	192	6923	57	4
	8.5	185	6282	60	4
	9.5	175	4771	62	3
	11	191	4951	76	3
	13	203	4716	79	2
	15	301	5646	72	3
	17	275	4154	104	2
	19	314	4380	119	4
	21	320	3947	125	3
	23	335	3481	130	2
	25	362	3824	140	3
GOF3 (R) Bottom water O$_2$ = 2.72 ml L^{-1}	0	87	6192	6	3
	0.5	80	6477	16	37
	1.5	195	6558	9	19
	2.5	303	6162	52	13
	3.5	372	5216	53	3
	4.5	563	4496	80	7
	6.5	667	2227	141	2
	8.5	776	953	194	1
	10.5	776	428	224	2
	12.5	871	444	260	4
	14.5	823	226	258	2
	17.5	799	1369	236	4
	20.5	1000	49	366	2
	23.5	1015	144	374	2
	26.5	1041	29	365	4
	29.5	1099	38	389	2

Core	Sample mid-depth (cm, 0 = bottom water)	NH$_4$	SO$_4$	HPO$_4$	Fe
GOF5 (R) Bottom water O$_2$ = 1.51 ml L^{-1}	0	11	7124	4	5
	0.5	64	7147	5	38
	1.5	68	7679	5	21
	2.5	122	7141	10	33
	3.5	148	6910	13	13
	4.5	160	6933	12	13
	6.5	221	5700	40	3
	8.5	328	5102	79	2
	10.5	422	3640	104	3
	12.5	451	3069	120	3
	14.5	507	2534	158	2
	17.5	585	1839	190	3
	20.5	583	1335	204	2
	23.5	629	1008	218	2
	26.5	589	760	189	2
	29.5	653	704	203	2
GOF6 (R) Bottom water O$_2$ = 0.89 ml L^{-1}	0	92	7263	33	1
	0.5	210	6428	161	2
	4.5	471	2615	177	4
	6.5	617	1292	188	2
	8.5	693	871	207	2
	12.5	907	488	294	2
	14.5	963	276	336	1
	16.5	1012	421	357	1
	18.5	1167	104	347	1
	20.5	1154	108	400	2
	24.5	1361	193	411	1
	26.5	1462	96	426	2
	28.5	1404	81	417	2
HBP115 (R) Bottom water O$_2$ = 0.00 ml L^{-1}	0	6	13108	2	4
	0.5	25	13056	27	59
	1.5	110	12748	88	71
	2.5	264	12155	70	32
	3.5	198	11940	75	11
	4.5	310	11725	89	4
	6.5	308	11224	98	1
	8.5	369	10781	114	1
	10.5	411	10411	125	1
	12.5	417	10277	121	1
	14.5	507	9534	133	1
	17.5	484	9259	150	1
	20.5	586	8233	173	1
	23.5	629	7722	182	1
	26.5	652	7448	184	1
	29.5	704	6993	193	1

Table A1. Continued.

Core	Sample mid-depth (cm, 0 = bottom water)	NH$_4$	SO$_4$	HPO$_4$	Fe
HBP136 (R)					
Bottom water	0	12	12338	4	7
O$_2$ = 0.16 ml L^{-1}	0.5	12	12536	9	20
	1.5	56	11930	64	74
	2.5	138	11946	93	92
	3.5	183	11751	97	81
	4.5	182	11706	84	67
	6.5	284	10923	127	21
	8.5	335	9159	166	2
	10.5	372	10289	166	2
	12.5	473	9058	228	2
	14.5	435	7041	238	1
	17.5	518	8146	244	2
	20.5	485	4858	302	1
	23.5	624	6919	301	1
	26.5	644	6427	312	1
	29.5	676	5937	320	2
HBP137 (R)					
Bottom water	0	10	12074	3	1
O$_2$ = 0.40 ml L^{-1}	0.5	12	12039	6	7
	1.5	34	11753	26	34
	2.5	86	11079	41	57
	3.5	121	10577	42	46
	4.5	167	10151	47	28
	6.5	206	10043	53	5
	8.5	281	9294	69	2
	10.5	317	9153	72	1
	12.5	334	8830	78	1
	14.5	346	8731	82	1
	17.5	336	8560	85	1
	20.5	322	8679	89	0
	23.5	305	8528	92	0
	26.5	284	8626	95	0
	29.5	271	8673	97	0

Core	Sample mid-depth (cm, 0 = bottom water)	NH$_4$	SO$_4$	HPO$_4$	Fe
HA2 (R)					
Bottom water	0	13	6907	5	0
O$_2$ = −1.44 ml L^{-1}	0.5	35	9499	8	0
	1.5	54	9240	10	0
	2.5	58	9164	11	0
	3.5	81	8917	15	0
	4.5	95	8876	17	0
	6.5	110	8703	19	0
	8.5	120	8538	22	0
	10.5	135	8459	25	0
	12.5	153	8276	29	0
	14.5	149	8507	27	0
	17.5	182	8350	34	0
	20.5	193	8334	37	0
	23.5	193	7985	38	0
	26.5	207	7717	42	0
	29.5	226	7544	45	0
	35.5	226	7371	50	0
	41.5	236	7314	54	0
	47.5	248	7227	55	0
LF3 (R)					
Bottom water	0	10	5874	4	0
O$_2$ = −0.13 ml L^{-1}	0.5	32	8727	7	0
	1.5	92	8092	17	0
	2.5	141	7606	27	0
	3.5	135	7707	26	0
	4.5	203	6949	42	0
	6.5	261	6691	53	0
	8.5	293	6061	65	0
	10.5	342	5744	73	0
	12.5	358	5419	81	0
	14.5	401	4974	90	0
	17.5	426	4619	90	0
	20.5	452	3989	102	0
	23.5	521	3708	119	0
	26.5	518	3531	124	0
	29.5	547	3803	116	0
	35.5	575	3063	131	0

Table B1. Solid-phase parameters, in $\mu\text{mol g}^{-1}$ salt-free dry sediment.

Core	Sample mid-depth (cm)	N_{tot}	C_{org}	Fe-P	P_{org}	Total P (ICP-OES)
BY2						
June	0.25	519	4745	41	13	69
	0.75	483	4493	45	13	68
	1.25	431	4040	66	12	80
	1.75	464	4374	72	11	75
	2.5	452	4272	27	7	53
	3.5	466	4397	25	11	51
	4.5	444	4243	11	12	36
	5.5	438	4159	11	10	37
	6.5	447	4257	13	11	40
	7.5	426	4098	7	10	34
	8.5	418	4062	7	11	34
	9.5	425	4111	7	10	36
	11	386	3720	5	10	32
	13	374	3638	4	9	30
	15	370	3598	4	9	30
	17	448	3939	3	9	29
	19	404	3861	4	9	28
	21	394	3848	4	9	30
	23	284	2807	4	9	31
	25	394	3905	5	10	30
	27	413	4068	4	9	31
	29	414	4104	5	10	33
LF1						
	0.25	257	2322		6	38
	0.75	235	2039		7	26
	1.25	211	1852		6	26
	1.75	214	1881		6	25
	2.5	183	1609		6	22
	3.5	129	1181		4	19
	4.5	97	887		4	17
	5.5	134	1228		4	19
	6.5	132	1224		4	18
	7.5	217	2006		6	21
	8.5	245	2262		7	22
	9.5	137	1292		5	19
	11	122	1176		4	19
	13	98	946		3	15
	15	84	821		3	17
	17	96	966		3	18
	19	73	733		3	16
	21	60	611		2	17
	23	84	888		3	17
	25	67	688		5	17
LF1.5						
	0.25	534	4943		11	46
	0.75	494	4119		9	34
	1.25	438	3787		9	33
	1.75	467	3974		10	36
	2.5	308	2680		8	28
	3.5	352	3024		7	29
	4.5	250	2171		6	24
	5.5	241	2033		6	23
	6.5	181	1572		5	21
	7.5	152	1367		5	20
	8.5	208	1894		5	21
	9.5	194	1754		6	20
	11	176	1629		5	22
	13	232	2164		6	25
	15	229	2136		6	23
	17	83	780		3	17
	19	107	997		3	17
	21	104	1005		3	19
	23	102	997		4	18
	25	199	1928		4	20
LF3						
	0.25	844	7948		19	54
	0.75	727	7101		14	43
	1.25	632	6158		10	36
	1.75	493	4669		13	32
	2.5	476	4524		15	31
	3.5	486	4570		11	31
	4.5	461	4357		12	31
	5.5	462	4309		9	30
	6.5	458	4331		12	30
	7.5	448	4360		12	29
	8.5	326	3054		8	26
	9.5	342	3260		9	26
	11	252	2296		7	23
	13	290	2683		7	24
	15	471	4584		12	30
	17	390	3809		9	27
	19	275	2511		7	24
	21	235	2082		8	22
	23	200	1713		5	23
	26	204	1770		5	22
	30	245	2225		7	24
F80						
	0.25	1133	11 690			
	0.75	1248	13 100		18	65
	1.25	1102	11 873		25	58
	1.75	1139	12 510		33	60
	2.5	1215	13 686		27	63
	3.5	1060	11 283			56
	4.5	968	9694		22	50
	5.5	733	7575		17	41
	6.5	790	8319		18	43
	7.5	840	8923		20	46
	8.5	733	7836		18	46
	9.5	732	7661		19	43
	11	734	7794		18	38
	13	728	7614		26	41
	15	665	6803		18	44
	17	677	6877		16	40
	19	721	7356		14	39
	21	644	6595		11	38

Table B1. Continued.

Core	Sample mid-depth (cm)	N_{tot}	C_{org}	Fe-P	P_{org}	Total P (ICP-OES)
	23	595	6296		15	38
	25	223	2448		7	36
	27	184	2122		6	36
	29	188	2152		9	44
	32	172	2170		8	30
LL19						
	0.25	906	9857		14	55
	0.75	1022	11376		17	58
	1.25	979	10721		19	55
	1.75	913	9729		16	51
	2.5	789	8180		16	43
	3.5	686	7357		14	41
	4.5	649	7031		14	40
	5.5	664	7055		12	44
	6.5	602	6326		11	41
	7.5	605	6443		13	39
	8.5	554	5983			
	9.5	282	3119		7	31
	11	204	2394		6	28
	13	172	2063		6	27
	15	153	1843		5	28
	17	147	1781		5	26
	19	147	1807		5	25
	21	137	1628		5	26
	23	142	1642		5	26
	25	137	1602		6	27

Core	Sample mid-depth (cm)	N_{tot}	C_{org}	Fe-P	P_{org}	Total P (ICP-OES)
BY15						
	0.25	896	9059		19	52
	0.75	959	9645		18	52
	1.25	752	7951		16	45
	1.75				18	41
	2.25	800	8244		19	40
	2.75	890	8862		16	40
	3.25	807	8425		18	37
	3.75	708	7129			
	4.25	829	7821		16	37
	5	479	5004		12	34
	6	347	3751		12	35
	7	296	3229		9	34
	8	241	2760		9	29
	9	257	3117		10	29
	10.5	220	2771		9	34
	12.5	227	2763		9	34
	14.5	237	2789		10	35
	16.5	219	2595			31
	18.5	233	2695		9	33
	20.5	254	2854		9	33
	22.5	252	2888		10	32
	24.5	232	2749		9	33
	26.5	220	2695		8	27
	29.5	252	2921		9	30
	33	300	3364		10	30
	35	316	3642		10	30
	36	315	3753		10	32
	37	323	3784		10	34
	38	346	3890		10	40
	39	314	3686		9	38

Table C1. Sediment solid phase parameters used in the calculation of ^{210}Pb-based age models.

Core	Sample mid-depth (cm)	Water content (wet sed., %)	Salt content (wet sed., %)*	Dry bulk density (dry, salt-free sed., g cm^{-3})	Cumulative mass at base of sample (g cm^{-2})	Observed ^{210}Pb activity (mBq g^{-1}, salt corr.)	Excess ^{210}Pb activity (mBq g^{-1}, salt corr.)**	Cumulative excess ^{210}Pb activity (mBq cm^{-2}, salt corr.)	Year (CRS model)	Mass accumulation rate (g cm^{-2} yr^{-1}, CRS model)
LF1										
	0.25	70.2	0.6	0.35	0.18	246.4	230.9	1001.00	2009.5	0.132
	0.75	68.1	0.5	0.38	0.37	261.0	245.5	960.20	2008.2	0.125
	1.25	65.8	0.5	0.42	0.58	250.4	234.9	913.01	2006.5	0.122
	1.75	64.4	0.5	0.44	0.80	240.4	224.9	863.50	2004.8	0.120
	2.5	63.6	0.5	0.46	1.26	222.5	207.0	813.49	2002.8	0.118
	3.5	50.3	0.4	0.71	1.97	147.0	131.5	718.77	1998.9	0.130
	4.5	44.1	0.3	0.85	2.82	117.8	102.3	625.58	1994.4	0.142
	5.5	48.7	0.4	0.74	3.56	117.5	102.0	538.92	1989.6	0.144
	6.5	51.1	0.4	0.69	4.25	109.7	94.2	463.29	1984.8	0.143
	7.5	59.3	0.5	0.53	4.78	305.6	290.1	398.11	1979.9	0.105
	8.5	62.4	0.5	0.48	5.26	151.4	135.9	243.59	1964.1	0.095
	9.5	55.6	0.4	0.60	5.86	99.4	83.9	178.53	1954.1	0.089
	11	55.2	0.4	0.61	7.08	89.9	74.4	128.05	1943.5	0.067
	13	43.0	0.3	0.87	8.83	33.2	17.7	37.40	1903.9	0.055
	15	40.9	0.3	0.92	10.67	16.0	0.5	6.49	1847.7	0.064
	17	42.7	0.3	0.88	12.43	18.6				
	19	39.5	0.3	0.96	14.35	15.2				
	21	37.7	0.3	1.01	16.37	15.9				
LF1.5										
	0.25	85.7	0.7	0.14	0.07	439.2	423.2	1299.11	2009.5	0.094
	0.75	84.2	0.7	0.16	0.15	474.2	458.2	1268.95	2008.7	0.089
	1.25	80.5	0.7	0.21	0.26	497.1	481.1	1232.09	2007.8	0.084
	1.75	78.9	0.6	0.23	0.37	412.8	396.8	1182.23	2006.5	0.086
	2.5	74.3	0.6	0.29	0.66	353.8	337.8	1136.81	2005.2	0.092
	3.5	74.1	0.6	0.30	0.96	344.4	328.4	1038.23	2002.3	0.092
	4.5	66.1	0.5	0.42	1.37	234.9	218.9	941.27	1999.2	0.101
	5.5	64.1	0.5	0.45	1.82	214.3	198.3	850.14	1995.9	0.106
	6.5	59.1	0.5	0.54	2.36	184.7	168.7	761.09	1992.3	0.111
	7.5	56.0	0.5	0.59	2.95	159.1	143.1	670.73	1988.3	0.115
	8.5	57.9	0.5	0.56	3.51	141.0	125.0	585.75	1983.9	0.118
	9.5	56.0	0.5	0.59	4.10	124.5	108.5	515.96	1979.8	0.121
	11	58.2	0.5	0.55	5.21	133.5	117.5	451.63	1975.6	0.116
	13	63.9	0.5	0.45	6.11	163.8	147.8	321.93	1964.7	0.098
	15	63.6	0.5	0.46	7.03	172.3	156.3	188.04	1947.4	0.065
	17	42.0	0.3	0.90	8.82	39.4	23.4	45.08	1901.6	0.045
	19	41.8	0.3	0.90	10.62	18.8	2.8	3.08	1815.4	
	21	45.2	0.4	0.82	12.26	15.9				
	23	45.6	0.4	0.81	13.88	14.2				
	25	57.8	0.5	0.56	15.00	17.0				
LF3										
	0.25	92.4	0.9	0.06	0.03	817.4	789.4	1078.93	2009.5	0.042
	0.75	92.1	0.9	0.07	0.06	744.0	716.0	1054.27	2008.8	0.044
	1.25	90.5	0.9	0.08	0.11	643.1	615.1	1030.68	2008.0	0.046
	1.75	87.1	0.9	0.12	0.17	499.6	471.6	1005.13	2007.2	0.052
	2.5	85.4	0.9	0.14	0.31	442.6	414.6	976.23	2006.3	0.059
	3.5	86.0	0.9	0.14	0.45	441.8	413.8	916.77	2004.3	0.061
	4.5	84.3	0.9	0.16	0.60	415.5	387.5	860.58	2002.2	0.063
	5.5	83.6	0.8	0.17	0.77	396.3	368.3	799.96	1999.9	0.063
	6.5	82.5	0.8	0.18	0.95	389.4	361.4	739.12	1997.4	0.063
	7.5	82.4	0.8	0.18	1.13	358.6	330.6	674.54	1994.4	0.062
	8.5	76.3	0.8	0.26	1.39	204.6	176.6	614.87	1991.4	0.068
	9.5	78.7	0.8	0.23	1.62	203.6	175.6	568.84	1988.9	0.071
	11	69.1	0.7	0.37	2.35	103.1	75.1	528.64	1986.6	0.089
	13	70.8	0.7	0.34	3.03	151.3	123.3	473.74	1983.1	0.093
	15	80.1	0.8	0.21	3.45	384.2	356.2	390.02	1976.8	0.072
	17	78.1	0.8	0.24	3.92	243.5	215.5	240.82	1961.3	0.060
	19	70.8	0.7	0.34	4.60	124.4	96.4	138.86	1943.7	0.053
	21	65.4	0.7	0.42	5.45	97.9	69.9	73.15	1923.1	0.039
	23	61.6	0.6	0.49	6.43	37.4	9.4	13.86	1869.7	
	26	61.9	0.6	0.48	8.36	27.7				

*Estimated from water content and bottom water salinity. **Assumed background (supported) ^{210}Pb concentrations (mBq g^{-1}): LF1: 15.5, LF1.5: 16.0, LF3: 27.0.

References

Algeo, T. J. and Ingall, E.: Sedimentary C-org : P ratios, paleocean ventilation, and Phanerozoic atmospheric pO_2, Palaeogeogr. Palaeocl., 256, 130–155, doi:10.1016/j.palaeo.2007.02.029, 2007.

Al-Hamdani, Z. and Reker, J.: Towards marine landscapes in the Baltic Sea, BALANCE interim report #10, available at: http://balance-eu.org/, 2007.

Boer, W., van den Bergh, G. D., de Haas, H., de Stigter, H. C., Gieles, R. and van Weering, T. C. E.: Validation of accumulation rates in Teluk Banten (Indonesia) from commonly applied Pb-210 models, using the 1883 Krakatau tephra as time marker, Mar. Geol., 227, 263–277, 2006.

Boudreau, B. P.: Diagenetic models and their implementation, Springer, Germany, 1997.

Burdige, D. J.: Geochemistry of marine sediments, Princeton University Press, New Jersey, USA, 2006.

Cardinale, M. and Modin, J.: Changes in size-at-maturity of Baltic cod (Gadus morhua) during a period of large variations in stock size and environmental conditions, Fish. Res., 41, 285–295, 1999.

Conley, D. J., Bjorck, S., Bonsdorff, E., Carstensen, J., Destouni, G., Gustafsson, B. G., Hietanen, S., Kortekaas, M., Kuosa, H., Meier, H. E. M., Muller-Karulis, B., Nordberg, K., Norkko, A., Nurnberg, G., Pitkanen, H., Rabalais, N. N., Rosenberg, R., Savchuk, O. P., Slomp, C. P., Voss, M., Wulff, F. and Zillen, L.: Hypoxia-related processes in the Baltic Sea, Environ. Sci. Technol., 43, 3412–3420, doi:10.1021/es802762a, 2009a.

Conley, D. J., Bonsdorff, E., Carstensen, J., Destouni, G., Gustafsson, B. G., Hansson, L. A., Rabalais, N. N., Voss, M. and Zillen, L.: Tackling hypoxia in the Baltic Sea: Is engineering a solution?, Environ. Sci. Technol., 43, 3407–3411, doi:10.1021/es8027633, 2009b.

Conley, D. J., Humborg, C., Rahm, L., Savchuk, O. P. and Wulff, F.: Hypoxia in the Baltic Sea and basin-scale changes in phosphorus biogeochemistry, Environ. Sci. Technol., 36, 5315–5320, doi:10.1021/es025763w, 2002.

de Lange, G. J., Thomson, J., Reitz, A., Slomp, C. P., Principato, M. S., Erba, E. and Corselli, C.: Synchronous basin-wide formation and redox-controlled preservation of a Mediterranean sapropel, Nat. Geosci., 1, 606–610, doi:10.1038/ngeo283, 2008.

Diaz, R. J. and Rosenberg, R.: Marine benthic hypoxia: A review of its ecological effects and the behavioural responses of benthic macrofauna, Oceanogr. Mar. Biol., 33, 245–303, 1995.

Einsele, W.: Über die Beziehungen des Eisenkreislaufs zum Phosphorkreislauf im eutrophen See, Arch. Hydrobiol., 29, 664–686,
1936.

Emeis, K. C., Struck, U., Leipe, T., Pollehne, F., Kunzendorf, H., and Christiansen, C.: Changes in the C, N, P burial rates in some Baltic Sea sediments over the last 150 years – relevance to P regeneration rates and the phosphorus cycle, Mar. Geol., 167, 43–59, 2000.

Emeis, K. C., Christiansen, C., Edelvang, K., Jahmlich, S., Kozuch, J., Laima, M., Leipe, T., Loffler, A., Lund-Hansen, L. C., Miltner, A., Pazdro, K., Pempkowiak, J., Pollehne, F., Shimmield, T., Voss, M., and Witt, G.: Material transport from the near shore to the basinal environment in the southern Baltic Sea II: Synthesis of data on origin and properties of material, J. Mar. Syst., 35, 151–168, 2002.

Fonselius, S.: Oxygen and hydrogen-sulfide conditions in the Baltic Sea, Mar. Pollut. Bull., 12, 187–194, 1981.

Fonselius, S. and Valderrama, J.: One hundred years of hydrographic measurements in the Baltic Sea, J. Sea Res., 49, 229–241, 2003.

Gustafsson, B. G.: Time-dependent modeling of the Baltic entrance area. 2. Water and salt exchange of the Baltic Sea, Estuaries, 23, 253–266, 2000.

Gustafsson, B. G. and Stigebrandt, A.: Dynamics of nutrients and oxygen/hydrogen sulfide in the Baltic Sea deep water, J. Geophys. Res.-Bio., 112, G02023, doi:10.1029/2006JG000304, 2007.

Hille, S.: New aspects of sediment accumulation and reflux of nutrients in the Eastern Gotland Basin (Baltic Sea) and its impact on nutrient cycling, Ph.D. thesis, Inst. of Biol., Rostock Univ., Rostock, Germany, 2005.

Hille, S., Nausch, G., and Leipe, T.: Sedimentary deposition and reflux of phosphorus (P) in the Eastern Gotland Basin and their coupling with P concentrations in the water column, Oceanologia, 47, 663–679, 2005.

Ingall, E. and Jahnke, R.: Influence of water-column anoxia on the elemental fractionation of carbon and phosphorus during sediment diagenesis, Mar. Geol., 139, 219–229, 1997.

Ingall, E. D., Bustin, R. M., and Van Cappellen, P.: Influence of water column anoxia on the burial and preservation of carbon and phosphorus in marine shales, Geochim. Cosmochim. Ac., 57, 303–316, 1993.

Intergovernmental Oceanographic Commission, International Hydrographic Organization and British Oceanographic Data Centre: Centenary Edition of the GEBCO Digital Atlas, published on CD-ROM on behalf of the Intergovernmental Oceanographic Commission and the International Hydrographic Organization as part of the General Bathymetric Chart of the Oceans, British Oceanographic Data Centre, Liverpool, U.K., 2003.

Janssen, F., Neumann, T., and Schmidt, M.: Inter-annual variability in cyanobacteria blooms in the Baltic Sea controlled by wintertime hydrographic conditions, Mar. Ecol.-Prog. Ser., 275, 59–68, 2004.

Jonsson, P., Carman, R., and Wulff, F.: Laminated sediments in the Baltic: A tool for evaluating nutrient mass balances, Ambio, 19, 152–158, 1990.

Karlson, K., Hulth, S., Ringdahl, K., and Rosenberg, R.: Experimental recolonisation of Baltic Sea reduced sediments: survival of benthic macrofauna and effects on nutrient cycling, Mar. Ecol.-Prog. Ser., 294, 35–49, 2005.

Kemp, W. M., Sampou, P., Caffrey, J., Mayer, M., Henriksen, K.,

and Boynton, W. R.: Ammonium recycling versus denitrification in Chesapeake Bay sediments, Limnol. Oceanogr., 35, 1545–1563, 1990.

Kraal, P., Slomp, C. P., and de Lange, G. J.: Sedimentary organic carbon to phosphorus ratios as a redox proxy in Quaternary records from the Mediterranean, Chem. Geol., 277, 167-177, doi:10.1016/j.chemgeo.2010.08.003, 2010.

Kraal, P., Slomp, C. P., Forster, A., Kuypers, M. M. M., and Sluijs, A.: Pyrite oxidation during sample storage determines phosphorus fractionation in carbonate-poor anoxic sediments, Geochim. Cosmochim. Ac., 73, 3277–3290, doi:10.1016/j.gca.2009.02.026, 2009.

Lass, H. U. and Matthaus, W.: On temporal wind variations forcing salt water inflows into the Baltic Sea, Tellus A, 48, 663–671, 1996.

Lilover, M. and Stips, A.: The variability of parameters controlling the cyanobacteria bloom biomass in the Baltic Sea, J. Mar. Syst., 74, S108–S115, doi:10.1016/j.jmarsys.2008.03.029, 2008.

Lukkari, K., Leivuori, M., and Kotilainen, A.: The chemical character and behaviour of phosphorus in poorly oxygenated sediments from open sea to organic-rich inner bay in the Baltic Sea, Biogeochemistry, 96, 25–48, doi:10.1007/s10533-009-9343-7, 2009.

Matthaus, W. and Franck, H.: Characteristics of major Baltic inflows – a statistical-analysis, Cont. Shelf Res., 12, 1375–1400, 1992.

Meier, H. E. M., Feistel, R., Piechura, J., Arneborg, L., Burchard, H., Fiekas, V., Golenko, N., Kuzmina, N., Mohrholz, V., Nohr, C., Paka, V. T., Sellschopp, J., Stips, A., and Zhurbas, V.: Ventilation of the Baltic Sea deep water: A brief review of present knowledge from observations and models, Oceanologia, 48, 133–164, 2006.

Middelburg, J. J. and Levin, L. A.: Coastal hypoxia and sediment biogeochemistry, Biogeosciences, 6, 1273–1293, doi:10.5194/bg-6-1273-2009, 2009.

Mort, H. P., Slomp, C. P., Gustafsson, B. G., and Andersen, T. J.: Phosphorus recycling and burial in Baltic Sea sediments with contrasting redox conditions, Geochim. Cosmochim. Ac., 74, 1350–1362, doi:10.1016/j.gca.2009.11.016, 2010.

Mortimer, C. H.: The exchange of dissolved substances between mud and water in lakes, J. Ecol., 29, 280–329, 1941.

Mortimer, C. H.: The exchange of dissolved substances between mud and water in lakes, J. Ecol., 30, 147–201, 1942.

Nausch, M., Nausch, G., Lass, H. U., Mohrholz, V., Nagel, K., Siegel, H., and Wasmund, N.: Phosphorus input by upwelling in the eastern Gotland Basin (Baltic Sea) in summer and its effects on filamentous cyanobacteria, Estuar. Coast. Shelf S., 83, 434–442, 2009.

Reed, D. C., Slomp, C. P., and Gustafsson, B. G.: Sedimentary phosphorus dynamics and the evolution of bottom water hypoxia: a coupled benthic-pelagic model of a coastal system, Limnol. Oceanogr., in press., 2011.

Ruttenberg, K. C.: Development of a sequential extraction method for different forms of phosphorus in marine sediments, Limnol. Oceanogr., 37, 1460–1482, 1992.

Savchuk, O. P., Wulff, F., Hille, S., Humborg, C., and Pollehne, F.: The Baltic Sea a century ago - a reconstruction from model simulations, verified by observations, J. Mar. Syst., 74, 485–494, doi:10.1016/j.jmarsys.2008.03.008, 2008.

Savchuk, O. P. and Wulff, F.: Long-term modeling of large-scale nutrient cycles in the entire Baltic Sea, Hydrobiologia, 629, 209–224, doi:10.1007/s10750-009-9775-z, 2009.

Schenau, S. J. and de Lange, G. J.: Phosphorus regeneration vs. burial in sediments of the Arabian Sea, Mar. Chem., 75, 201–217, 2001.

Schinke, H. and Matthaus, W.: On the causes of major Baltic inflows – an analysis of long time series, Cont. Shelf Res., 18, 67–97, 1998.

Seeberg-Elverfeldt, J., Schluter, M., Feseker, T., and Kolling, M.: Rhizon sampling of porewaters near the sediment-water interface of aquatic systems, Limnol. Oceanogr.-Meth., 3, 361–371, 2005.

Slomp, C. P., Epping, E. H. G., Helder, W., and Van Raaphorst, W.: A key role for iron-bound phosphorus in authigenic apatite formation in North Atlantic continental platform sediments, J. Mar. Res., 54, 1179–1205, 1996.

Slomp, C. P., Malschaert, J. F. P., and Van Raaphorst, W.: The role of adsorption in sediment-water exchange of phosphate in North Sea continental margin sediments, Limnol. Oceanogr., 43, 832–846, 1998.

Slomp, C. P., Thomson, J., and de Lange, G. J.: Enhanced regeneration of phosphorus during formation of the most recent eastern Mediterranean sapropel (S1), Geochim. Cosmochim. Ac., 66, 1171–1184, 2002.

Stigebrandt, A.: Computations of oxygen fluxes through the sea-surface and the net production of organic-matter with application to the Baltic and adjacent seas, Limnol. Oceanogr., 36, 444–454, 1991.

Strickland, J. D. and Parsons, T. R.: A practical handbook of seawater analysis, Bulletin 167, Fisheries Research Board of Canada, Ottawa, Canada, 1972.

Struck, U., Pollehne, F., Bauerfeind, E. and Bodungen, B. V.: Sources of nitrogen for the vertical particle flux in the Gotland Sea (Baltic Proper) – results from sediment trap studies, J. Mar. Syst., 45, 91–101, doi:10.1016/j.jmarsys.2003.11.012, 2004.

Turnewitsch, R. and Pohl, C.: An estimate of the efficiency of the iron- and manganese-driven dissolved inorganic phosphorus trap at an oxic/euxinic water-column redoxcline, Global Biogeochem. Cy., 24, GB4025, doi:10.1029/2010GB003820, 2010.

Vahtera, E., Conley, D. J., Gustafsson, B. G., Kuosa, H., Pitkanen, H., Savchuk, O. P., Tamminen, T., Viitasalo, M., Voss, M., Wasmund, N., and Wulff, F.: Internal ecosystem feedbacks enhance nitrogen-fixing cyanobacteria blooms and complicate management in the Baltic Sea, Ambio, 36, 186–194, 2007.

Van Cappellen, P. and Ingall, E. D.: Response to comment "Redox stabilization of the atmosphere and oceans and marine productivity" edited by: Colman, A. S., Mackenzie, F. T., and Holland, H. D., Science, 275, 407–408, 1997.

Van Cappellen, P. and Wang, Y.: Metal cycling in sediments: Modeling the interplay of reaction and transport, in: Metal contaminated aquatic sediments, edited by: Allen, H. E., Ann Arbor Press, Michigan, USA, 1995.

Van Santvoort, P. J. M., De Lange, G. J., Thomson, J., Colley, S., Meysman, F. J. R., and Slomp, C. P.: Oxidation and origin of organic matter in surficial eastern Mediterranean hemipelagic sediments, Aquat. Geochem., 8, 153–175, 2002.

Zillén, L., Conley, D. J., Andrén, T., Andrén, E., and Björck, S.: Past occurrences of hypoxia in the Baltic Sea and the role of climate variability, environmental change and human impact, Earth Sci. Rev., 91, 77–92, 2008.